

TPR-97-07

Fine-Tuning Two-Particle Interferometry: Effects from Opacity and Temperature Gradients in the Source

Boris Tomášik and Ulrich Heinz

*Institut für Theoretische Physik, Universität Regensburg,
D-93040 Regensburg, Germany*

July 1, 1997

Abstract

A comprehensive model study of Bose-Einstein correlation radii in heavy ion collisions is presented. The starting point is a longitudinally and transversally expanding fireball, represented at freeze-out by an azimuthally symmetric emission function. The freeze-out temperature is allowed to feature transverse and temporal gradients. Their effects on the correlation radii are studied. In particular, we evaluate numerically their dependence on the transverse mass of the particle pairs and check a recent suggestion, based on analytical approximations, that for certain reasonable source parameters all three correlation radii satisfy simultaneously a $1/\sqrt{M_\perp}$ scaling. We also investigate quantitatively how the correlation radii are affected if the source becomes “opaque”. We find a strong sensitivity to opaqueness for the temporal radius parameter R_0 in the YKP parametrization. A qualitative comparison with preliminary data from 158 A GeV/c Pb+Pb collisions at CERN indicates that the source is not opaque, but rather transparent. For opaque sources we find some regions of inapplicability of the YKP parametrization which can be avoided by a slightly different parametrization for the correlator. The physical meaning of the modified parameters is briefly discussed.

1 Introduction

Recently, two-particle intensity interferometry, exploiting the effects of Bose-Einstein (BE) symmetrization on the two-particle momentum spectra, has been developed into a powerful tool for measuring not only the space-time dimensions of the particle emitting object, but also its dynamical state at particle freeze-out. Modern Bose-Einstein interferometry thus goes far beyond the original work by Hanbury Brown and Twiss, who introduced and successfully demonstrated photon intensity interferometry for static sources in astrophysics [1], and the pioneering paper by Goldhaber, Goldhaber, Lee, and Pais [2] who first exploited similar ideas in particle physics. Good reviews of the basic theoretical and experimental techniques can be found in Refs. [3, 4, 5, 6, 7] while the more recent theoretical developments are summarized in a series of lectures published in Ref. [8].

Collective dynamics of the source leads to a characteristic dependence of the two-particle correlation function on the total momentum of the particle pair. The width of the correlator as a function of the relative momentum of the two particles measures the size of the “regions of homogeneity” [9] inside the source across which the momentum distribution changes sufficiently little to guarantee measurable rates for pairs with similar momenta of the two particles. For rapidly expanding sources widely separated points do not emit particles of similar momenta; the homogeneity regions seen by BE correlation function thus form only a fraction of the whole source. Moreover, the momentum of a particle defines the homogeneity region from which it is coming; we will call the homogeneity region which contributes to the emission of particles with a given momentum the “effective source” for such particles.

The size parameters of the “effective source” (which are measured by the correlator and which we will thus call “correlation radii” or simply “HBT radii”) are related to the magnitude of the velocity gradients in the source, multiplied with a thermal smearing factor $\sqrt{T/M_{\perp}}$ originating from the local momentum distribution [10, 11, 12]. They are thus affected by both the expansion velocity profile of the source and by variations of the width (“temperature”) of the local momentum distributions across the source [11, 13, 14, 15, 16]. Another physical mechanism which can, even in the absence of flow and temperature gradients, lead to dramatic differences between the “effective source” of particles with a fixed momentum K and the momentum-integrated distribution of source points in space-time is strong reabsorption or rescattering of the particles in the interior of the source; this leads to a surface-dominated distribution of last interaction points with a strong preference for outward-directed momenta. Such “opaque sources” and their effects on the correlation radii have recently been discussed in Refs. [17, 18] on a semianalytic level using simple models.

While the basic relations between such source features as mentioned above and the properties of the measurable two-particle correlation functions appear to be qualitatively understood, this is not sufficient for a quantitative interpretation of two-particle correlation data and a complete reconstruction of the source from the measurements. Quantitative numerical investigations, including comprehensive parameter studies, so far exist mostly for transparent expanding sources with constant freeze-out temperature [12, 19, 20, 21], while for sources with temperature gradients some numerical checks of the approximate analytical approximations developed in [13, 14, 15] have been performed in Refs. [22, 23]. In [22] the validity range of the analytical formulae

given in Ref. [14] was determined. A comparison with experimental data from 200 A GeV/ c S+Pb collisions [24] in Ref. [23] revealed, however, that the required source parameters lie outside this range of validity. A quantitative comparison with data thus requires numerical studies.

The purpose of the present paper is two-fold: In the first part we present a numerical parameter study of the influence of flow and temperature gradients on the correlation radii. One goal of this investigation is to settle a question which was left open in Refs. [22, 23]: based on a series of approximations, the authors of Ref. [14] had found a common $1/\sqrt{M_\perp}$ scaling law for all three HBT radii R_s , R_o , R_l in a Cartesian parametrization of the correlator. This was desirable in view of the S+Pb data of Ref. [24] where agreement with such a common scaling law was reported (although supported only by three data points in each Cartesian direction). The data of Refs. [25, 26, 27, 28, 29, 30] from S+S, S+Ag, S+Au, and Pb+Pb collisions, on the other hand, all show a much stronger M_\perp -dependence of the longitudinal HBT radii compared to the transverse ones. This is in qualitative agreement with the theoretical studies in Refs. [12, 19, 20] which, for sources with constant temperature and boost-invariant longitudinal, but weaker transverse expansion, show a weaker M_\perp -dependence for R_s than for R_l . In [12, 20] it was argued that, if one fits the M_\perp -dependence of the HBT radii with a negative power law, $R_i(M_\perp) \sim M_\perp^{-\alpha_i}$ [26, 27, 30], the power α_i itself should be proportional to the rate of expansion in direction i ; this feature cannot be obtained within the simple saddle point approximation used in Refs. [10, 11, 13, 14, 16, 31]. We show here that, within the phenomenologically allowed parameter range, this remains true even in the presence of temperature gradients.

In contrast to the work of Refs. [22, 23] we also compute the HBT radii in the Yano-Koonin-Podgoretskii (YKP) parametrization of the correlation function [32, 33, 31] which have a more straightforward and simpler interpretation in space-time [31, 20] than the HBT parameters from the Cartesian (Pratt-Bertsch-Chapman) parametrization [10, 11]. As far as we know, the effects of temperature gradients on the YKP parameters have not been studied before.

The second part of our investigation deals with opacity effects. Surface dominated, “opaque” sources typically emit particles from a thin shell near the surface of the fireball and are thus characterized by a smaller space-time extension in the “outward” (x) than in the “sideward” (y) direction, $\langle \tilde{x}^2 - \tilde{y}^2 \rangle < 0$. (The tilde notation will be defined in the next Section; it indicates that we are talking about the corresponding variances of the distribution of emission points in space-time). This is in particular true [34] for typical emission functions from hydrodynamical simulations where freeze-out is implemented along a sharp hypersurface, characterized e.g. by a constant temperature, while for transparent sources of the type studied e.g. in [14, 31, 20] the difference $\langle \tilde{x}^2 - \tilde{y}^2 \rangle$ is positive and small.

In Refs. [17, 18] it was pointed out that this feature of opaque sources generally leads to smaller values for R_o than for R_s in the Cartesian parametrization of the correlator. In particular for pairs with vanishing transverse momentum $K_\perp = 0$, one has [10] $R_s^2 = \langle \tilde{y}^2 \rangle > R_o^2 = \langle \tilde{x}^2 \rangle$ if $\langle \tilde{x}^2 - \tilde{y}^2 \rangle < 0$. The existence of a thin emission layer with directed emission only into the outward hemisphere thus breaks the usual symmetry argument [31, 12] that $\lim_{K_\perp \rightarrow 0} (R_o^2 - R_s^2) = 0$. That argument is based on the assumed azimuthal symmetry of the effective source for vanishing K_\perp where the direction of the transverse pair momentum no longer serves to distinguish between

the outward and sideward directions (parallel and perpendicular to \mathbf{K}_\perp); for opaque sources the orientation of the emitting surface itself provides that distinction.

Here we show that in the YKP parametrization the opacity effects get enhanced in the “temporal” radius parameter R_0^2 which turns negative for small K_\perp and diverges to minus infinity in the limit $K_\perp \rightarrow 0$ if $\langle \tilde{x}^2 - \tilde{y}^2 \rangle < 0$. While this would destroy an interpretation of R_0 in terms of the effective source lifetime, it would provide particularly clear evidence for surface dominated emission. Since no such evidence is seen in the preliminary data from the NA49 Collaboration who presented a YKP-analysis of the correlation functions from Pb+Pb collisions at the Quark Matter '96 conference [28], rather stringent limits on the degree of “opaqueness” of the source created in these collisions can already now be established (see Sec. 5.2).

In the course of this study we discovered that for opaque sources the YKP parametrization may become ill-defined in certain kinematic regions. In Sec. 5.3 we establish a modification of the YKP parametrization without this defect. The cost for the remedy is a less straightforward physical interpretation of its radius parameters. Fortunately, for transparent sources the YKP parametrization generally appears to work well.

We want to stress that resonance decays are not addressed in this paper. It is known that they can strongly affect the correlation function [35, 36, 37, 38, 39, 40] in which case a Gaussian parametrization as employed here becomes questionable [40, 41, 42]. Thus, while our calculations refer both to pion and kaon correlations, only the kaon results and those for high- K_\perp pions (where resonance decays can be neglected) can be directly related to data. For low- K_\perp pion pairs our results show the features of the contribution from directly emitted pions to the correlator.

2 Formalism

For chaotic sources the two-particle correlation function is in very good approximation given by the formula [43, 44, 45]

$$C(q, K) \simeq 1 + \frac{|\int d^4x S(x, K) e^{iq \cdot x}|^2}{|\int d^4x S(x, K)|^2}. \quad (1)$$

Here $S(x, K)$ is the emission function (single-particle Wigner phase-space density) of the source [43, 44, 45], and $K = \frac{1}{2}(p_1 + p_2)$ (with $p_{1,2}$ on-shell) is the average pair momentum while $q = p_1 - p_2$ denotes the momentum difference between the two particles.

One usually parameterizes the correlation function by a Gaussian in q [19, 20]. Since q satisfies the on-shell constraint $q \cdot K = 0$, only three of its four components are independent. This leaves room for various (mathematically equivalent) Gaussian parametrizations, using different sets of independent q -components. Here we will consider only azimuthally symmetric sources and evaluate the parameters (HBT radii) of the Cartesian and of the Yano-Koonin-Podgoretskii (YKP) parametrizations, in the commonly used coordinate system where the z axis defines the beam direction and \mathbf{K} lies in the $x - z$ plane. The x axis is customarily labeled as o (for *outward*), y as s (for *sideward*), and z as l (for *longitudinal*).

The Cartesian parametrization of the correlator employs the three spatial compo-

nents of q in the form [10, 11]

$$C(\mathbf{q}, \mathbf{K}) = 1 + \exp \left[-R_s^2(\mathbf{K})q_s^2 - R_o^2(\mathbf{K})q_o^2 - R_l^2(\mathbf{K})q_l^2 - 2R_{ol}^2(\mathbf{K})q_oq_l \right]. \quad (2)$$

The four \mathbf{K} -dependent parameters (HBT radii) are then given by linear combinations of the space-time variances of the effective source of particles with momentum¹ K [10, 11, 46]:

$$R_s^2(\mathbf{K}) = \langle \tilde{y}^2 \rangle, \quad (3)$$

$$R_o^2(\mathbf{K}) = \langle (\tilde{x} - \beta_{\perp}\tilde{t})^2 \rangle, \quad (4)$$

$$R_l^2(\mathbf{K}) = \langle (\tilde{z} - \beta_l\tilde{t})^2 \rangle, \quad (5)$$

$$R_{ol}^2(\mathbf{K}) = \langle (\tilde{x} - \beta_{\perp}\tilde{t})(\tilde{z} - \beta_l\tilde{t}) \rangle. \quad (6)$$

The angular brackets denote space-time averages taken with the emission function $S(x, K)$ of the effective source at momentum K , and coordinates with a tilde are measured relative to the center of the effective source: $\tilde{x}_{\mu} = x_{\mu} - \bar{x}_{\mu}$, $\bar{x}_{\mu} = \langle x_{\mu} \rangle$ [19].

In the LCMS (Longitudinally CoMoving System [47]), where $\beta_l = K_l = 0$, R_l^2 and R_{ol}^2 simplify to

$$R_l^2 = \langle \tilde{z}^2 \rangle, \quad (7)$$

$$R_{ol}^2 = \langle (\tilde{x} - \beta_{\perp}\tilde{t})\tilde{z} \rangle. \quad (8)$$

For further discussions of these expressions see [10, 11].

The YKP parametrization employs the components q^0 , $q_{\perp} = \sqrt{q_o^2 + q_s^2}$, and q_l in the form [31, 19, 20]

$$C(\mathbf{q}, \mathbf{K}) = 1 + \exp \left[-R_{\perp}^2(\mathbf{K})q_{\perp}^2 - R_{\parallel}^2(\mathbf{K})\left(q_l^2 - (q^0)^2\right) - \left(R_0^2(\mathbf{K}) + R_{\parallel}^2(\mathbf{K})\right)(q \cdot U(\mathbf{K}))^2 \right]. \quad (9)$$

The YKP radii R_{\perp} , R_{\parallel} , and R_0 are invariant under longitudinal boosts of the measurement frame; they measure (in some approximation) the transverse, longitudinal, and temporal extension of the effective source in its longitudinal rest frame (called Yano-Koonin (YK) frame) [31, 19, 20]. This frame moves with the YK velocity $v(\mathbf{K})$, defined by the fourth fit parameter $U(\mathbf{K})$ via

$$U(\mathbf{K}) = \gamma(\mathbf{K})(1, 0, 0, v(\mathbf{K})), \quad \gamma(\mathbf{K}) = \frac{1}{\sqrt{1 - v^2(\mathbf{K})}}. \quad (10)$$

The YKP parameters can be calculated from the emission function through relations similar to (3)-(6): Defining [19, 20]

$$A = \left\langle \left(\tilde{t} - \frac{\tilde{\xi}}{\beta_{\perp}} \right)^2 \right\rangle, \quad (11)$$

$$B = \left\langle \left(\tilde{z} - \frac{\beta_l}{\beta_{\perp}}\tilde{\xi} \right)^2 \right\rangle, \quad (12)$$

$$C = \left\langle \left(\tilde{t} - \frac{\tilde{\xi}}{\beta_{\perp}} \right) \left(\tilde{z} - \frac{\beta_l}{\beta_{\perp}}\tilde{\xi} \right) \right\rangle, \quad (13)$$

¹We denote the dependence on the pair momentum alternatively by \mathbf{K} or K where in the latter case the on-shell approximation $K^0 = \sqrt{m^2 + \mathbf{K}^2}$ is implied.

with $\tilde{\xi} \equiv \tilde{x} + i\tilde{y}$ such that $\langle \tilde{\xi}^2 \rangle = \langle \tilde{x}^2 - \tilde{y}^2 \rangle$, they are given by²

$$v = \frac{A+B}{2C} \left(1 - \sqrt{1 - \left(\frac{2C}{A+B} \right)^2} \right), \quad (14)$$

$$R_{\parallel}^2 = B - vC, \quad (15)$$

$$R_0^2 = A - vC, \quad (16)$$

$$R_{\perp}^2 = \langle \tilde{y}^2 \rangle. \quad (17)$$

Note that the Yano-Koonin velocity v , and thus R_{\parallel} and R_0 , are well-defined only for effective sources with $(A+B)^2 - 4C^2 \geq 0$. As shown in Appendix A and further discussed in Sec. 5 this condition can be violated in particular for opaque sources. In the limit $C \rightarrow 0$ the YK velocity v vanishes such that this condition defines the YK frame. In this frame $R_{\parallel}^2 = B$ and $R_0^2 = A$.

As a side remark, we would like to note that the quantities A, B, C from Eqs. (11)-(13) are identical with the radius parameters introduced in Refs. [21, 40, 42], where a different Cartesian parametrization based on the same q -components as in the YKP case was used:

$$C(\mathbf{q}, \mathbf{K}) = 1 + \exp[-R_{\perp}^2(\mathbf{K})q_{\perp}^2 - R_z^2(\mathbf{K})q_l^2 - R_t^2(\mathbf{K})(q^0)^2 - 2R_{zt}^2(\mathbf{K})q_lq^0]. \quad (18)$$

One easily shows

$$R_t^2 = A, \quad R_z^2 = B, \quad R_{zt}^2 = -C. \quad (19)$$

Clearly, these parameters are not boost-invariant and thus don't lead directly to a simple space-time interpretation of the correlator. Their usefulness is rather of technical nature in the actual data fitting procedure [21, 40, 42] and, of course, the YKP parameters can be reconstructed from them via Eqs. (14)-(16).

Our calculations in the following Sections of the correlation radii will be based on the expressions (3)-(8) and (11)-(17).

3 Hydrodynamic parametrization of the source

For our studies we use a generalization of the model of Ref. [14], including an exponential damping factor to parametrize “opaqueness” [17, 18]:

$$\begin{aligned} S(x, K) d^4x &= \frac{M_{\perp} \cosh(\eta - Y)}{(2\pi)^3} \exp\left[-\frac{K \cdot u(x)}{T(x)}\right] \exp\left[-\frac{r^2}{2R^2} - \frac{(\eta - \eta_0)^2}{2(\Delta\eta)^2}\right] \\ &\times \exp\left[-\kappa \frac{l_{\text{eff}}}{\lambda}\right] \frac{\tau d\tau}{\sqrt{2\pi(\Delta\tau)^2}} \exp\left[-\frac{(\tau - \tau_0)^2}{2(\Delta\tau)^2}\right] d\eta r dr d\phi. \end{aligned} \quad (20)$$

This “emission function” parametrizes the distribution of points of last interaction in the source. The parametrization (20) is motivated by hydrodynamical models with approximately boost-invariant longitudinal dynamics. It uses thermodynamic and hydrodynamic parameters and appropriate coordinates; for a detailed discussion see, e.g.,

²Please note that the first expressions given on the r.h.s of Eqs. (19b,c) in Ref. [19] are only valid if $A + B \geq 0$.

[8]. In the calculations we use the on-shell approximation $K_0 \approx E_K = \sqrt{m^2 + \mathbf{K}^2}$ as discussed in [11].

The velocity field $u(x)$ determines the dynamics of the source at freeze-out. We parametrize it by [12]

$$u^\mu(x) = (\cosh \eta \cosh \eta_t(r), \cos \phi \sinh \eta_t(r), \sin \phi \sinh \eta_t(r), \sinh \eta \cosh \eta_t(r)), \quad (21)$$

thereby implementing a boost-invariant longitudinal flow profile $v_L = z/t$, with a linear radial profile of strength η_f for the transverse flow rapidity³:

$$\eta_t(r) = \eta_f \frac{r}{R}. \quad (22)$$

Parameterizing K in the usual way through rapidity Y , transverse mass M_\perp and transverse momentum K_\perp , the exponent of the Boltzmann term reads

$$K \cdot u(x) = M_\perp \cosh(\eta - Y) \cosh \eta_t(r) - K_\perp \sinh \eta_t(r) \cos \phi. \quad (23)$$

For $\eta_f = 0$ the emission function depends only on M_\perp and not on K_\perp . This scaling is broken by the transverse flow.

A special feature of the model suggested in [14] is the following parametrization of the temperature profile:

$$\frac{1}{T(x)} = \frac{1}{T_0} \left(1 + a^2 \frac{r^2}{2R^2} \right) \left(1 + d^2 \frac{(\tau - \tau_0)^2}{2\tau_0^2} \right). \quad (24)$$

It introduces transverse and temporal temperature gradients which are scaled by the parameters a and d . Such a profile concentrates the production of particles with large M_\perp near the symmetry axis and close to the average freeze-out time [14, 15]. Note that the space-time dependence of the temperature does not break the M_\perp -scaling of the emission function in the absence of transverse flow.

Following [17, 18] the factor $\exp[-\kappa(l_{\text{eff}}/\lambda)]$ was introduced into the emission function to implement a possible opaqueness of the source. A particle emitted at point (r, ϕ) and travelling in outward (x) direction towards the detector has a probability for arriving there unscattered which decreases exponentially with its effective travelling distance through matter:

$$l_{\text{eff}} = l_{\text{eff}}(r, \phi) = e^{-\frac{y^2}{2R^2}} \int_x^\infty e^{-\frac{x'^2}{2R^2}} dx' \quad \text{with} \quad y = r \sin \phi, \quad x = r \cos \phi. \quad (25)$$

The Gaussians in this expression parametrize the matter density seen by the particle according to the source distribution (20). λ is the particle's mean free path (called λ_{mfp} in [17]); as $\lambda \rightarrow \infty$ we recover the transparent source of Ref.[14]. The constant $\kappa = \sqrt{8/\pi}$ is chosen in such a way that particles produced at the symmetry axis suffer the same suppression here as in the model of Heiselberg and Vischer [17] once the rms radius of the source is adjusted to the same value in both models. (In [17] a box profile was used for the transverse density distribution.) Note, however, that contrary to [18] our opaqueness parameter λ and transverse geometric radius R are time-independent.

³The nonrelativistic approximation of this transverse profile used in [11, 14, 31] is advantageous for analytic manipulations but not necessary if the correlation radii are evaluated numerically.

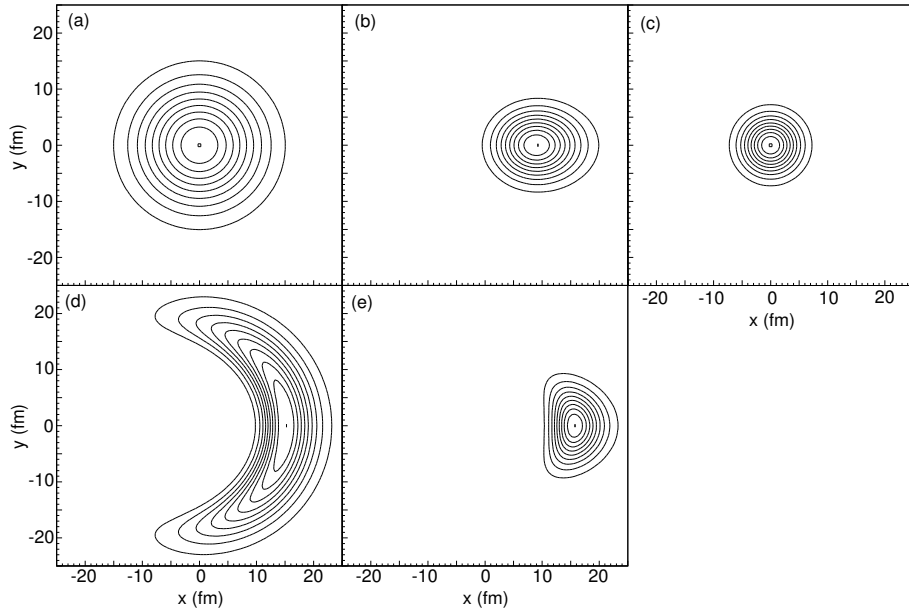


Figure 1: Transverse cuts of the emission function for midrapidity pions with transverse momentum $K_\perp = 500$ MeV/c (in x -direction), for the model parameters given in Table 1. Top row (a-c): transparent sources ($\lambda = \infty$); bottom row (d,e): opaque sources with $\lambda = 0.5$ fm. Left column (a,d): neither flow nor temperature gradients; middle column (b,e): transverse flow only with $\eta_f = 0.7$; right column (c): transverse temperature gradient only with $a = 0.8$.

The emission functions (effective sources for pions with given momenta) for different model parameters are shown as density contour plots in Figs. 1 and 2. Transverse cuts of the emission function are displayed in Fig. 1. When switching on the opaqueness, the transverse size of the effective source is seen to increase dramatically (cf. Figs. 1a,d); this is due to the suppression factor $\exp[-\kappa(l_{\text{eff}}/\lambda)]$ which cuts out all of the interior of the source and leaves only the right hemisphere of the dilute tail of the Gaussian transverse density distribution (outside of the lowest density contour in Fig. 1a). This cannot happen in the model of Heiselberg and Vischer [17] who use a transverse box profile without Gaussian tails. For a source with the shape given in Fig. 1d the Gaussian approximation, on which the expressions of Sec. 2 are based with which we evaluate the HBT radii, may become questionable; for a qualitative understanding of the relevant features it should, however, be still sufficient.

Transverse flow is seen to decrease the effective source more in the sideward than in the outward direction (see Figs. 1b,d and also Fig. 3 in [12]); this is particularly true for opaque sources (cf. Figs. 1d,e). Transverse temperature gradients, on the other hand, just reduce the homogeneity lengths without changing the shape of the source (cf. Figs. 1a,c).

A temporal temperature gradient has no impact on the transverse source profile; its effect on the longitudinal profile is seen in Fig. 2 (top vs. bottom row) where it

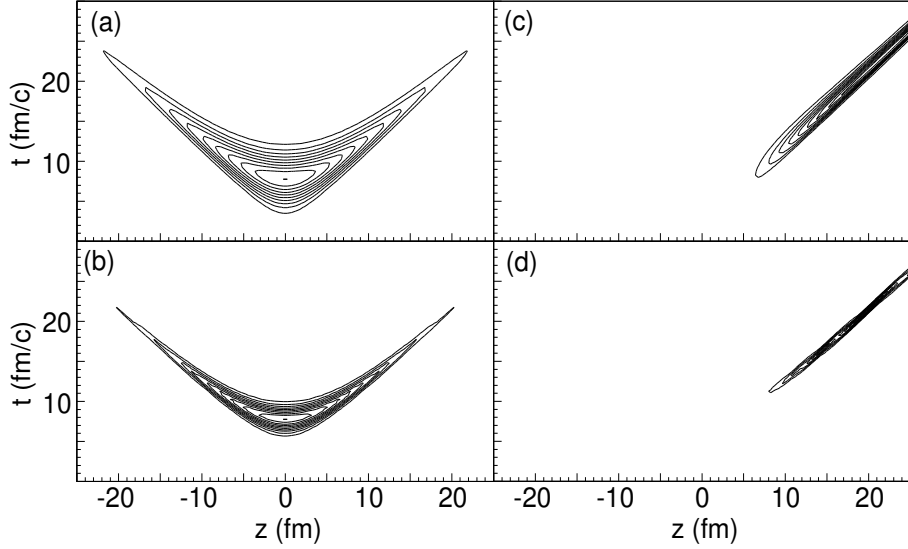


Figure 2: Contour plots of the $z - t$ profiles of the emission function for pions. The profiles are calculated in the CMS. (a,b): pair rapidity $Y = 0$, transverse pair momentum $K_{\perp} = 1$ MeV/c. (c,d): $Y = 2$, $K_{\perp} = 500$ MeV/c. The sensitivity of the profiles to K_{\perp} is weak. Source parameters as given in Table 1, $\eta_f = a = 0$. Upper row (a,c): no temporal temperature gradient, $d = 0$; lower row (b,d): $d = 1.5$.

decreases the temporal width of the effective sources without otherwise changing the shape of the emission function.

Fig. 2 also shows the different shapes of the effective source in the center of mass system (CMS) of the fireball for midrapidity and forward rapidity pions. An interesting feature are the emission time distributions: one clearly sees that the boost-invariant longitudinal expansion and proper-time freeze-out leads to freeze-out at different times in different places and thus generates time distributions in a fixed coordinate system which cover a much larger region [12, 19] than the one corresponding to the intrinsic eigentime width encoded in the emission function (20). The strongly non-Gaussian shape of the longitudinal source distribution is known [12] to lead to non-Gaussian effects on the longitudinal correlator; as shown in [40] its Gaussian shape is, however, to some extent restored by resonance decay contributions (not considered here) which fill in the central region above the “hyperbola” in the thermal source shown in Figs. 2a,b.⁴

For our numerical model study we use, if not stated otherwise, the source (20) with the model parameters listed in Table 1.

⁴We thank to Urs Wiedemann for making this point.

Table 1: Values of model parameters used in numerical calculations.

temperature T_0	100 MeV
average freeze-out proper time τ_0	7.8 fm/ c
mean proper emission duration $\Delta\tau$	2 fm/ c
geometric (Gaussian) transverse radius R	7 fm
Gaussian width of the space-time rapidity profile $\Delta\eta$	1.3
pion mass m_{π^\pm}	139 MeV/ c^2
kaon mass m_{K^\pm}	493 MeV/ c^2

4 Influence of temperature and flow gradients on the HBT radii of a transparent source

In this Section we discuss the effects of various types of gradients in the source on the correlation radii. To be able to recognize their specific signals we first investigate the correlation radii in the absence of transverse flow and temperature gradients. At the end of this Section we try with the help of temperature gradients to reproduce the $1/\sqrt{M_\perp}$ scaling proposed in Ref.[14] for R_s and the emission duration.

For the sake of clarity, let us list here the various reference frames which will appear in the following discussion. They differ by their longitudinal velocities.

CMS Center of Mass System of the fireball. In this frame $\eta_0 = 0$.

LCMS Longitudinally Co-Moving System – a frame moving longitudinally with the particle pair, i.e., $Y = 0$, $\beta_l = 0$.

YK The Yano-Koonin frame. It moves longitudinally with the Yano-Koonin velocity v . The YKP radii measure the homogeneity lengths of the source in this frame.

LSPS Longitudinal Saddle-Point System. This frame moves longitudinally with the point where the emission function for particles with a given momentum K has its maximum (point of maximal emissivity).

It is obvious that each particle pair (via its momentum K) defines its own LCMS, YK, and LSPS frame. The rapidity of the pair in the CMS will be denoted by $Y_{\text{CM}} = Y - \eta_0$.

4.1 No temperature and flow gradients

In Fig. 3 we show the M_\perp dependence of the correlation radii for both the Cartesian and Yano-Koonin-Podgoretskii parametrizations, for a source without transverse flow and temperature gradients. Non-trivial M_\perp dependencies thus results solely from the effects of longitudinal expansion or have a kinematic origin. All HBT radii are calculated from space-time variances of the emission function evaluated in the LCMS. These curves are shown for later reference only; for a detailed interpretation of their features we refer to the existing literature [9, 12, 31, 19, 20, 11]. Here we concentrate on a few relevant features:

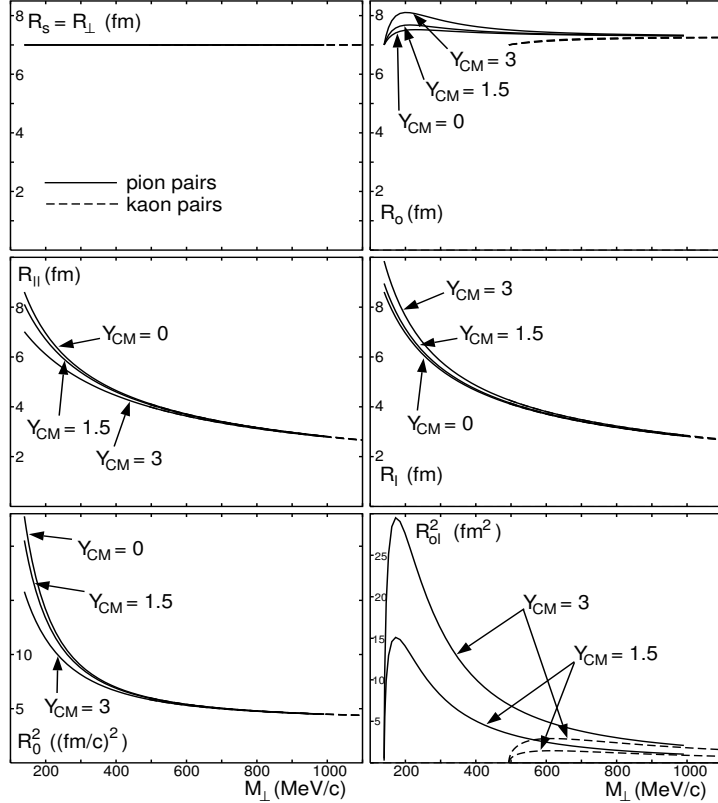


Figure 3: Correlation radii in the absence of temperature gradients and transverse flow, calculated for a transparent source with model parameters from Table 1. In the left (right) column the M_\perp dependences of the YKP (Cartesian) radii are shown. The space-time variances from which they are calculated are evaluated in the LCMS. The HBT radii for pions (kaons) are shown as solid (dashed) lines, in three rapidity regions: $Y_{CM} = 0$, $Y_{CM} = 1.5$ and $Y_{CM} = 3$.

Due to the absence of transverse gradients, $R_s = R_\perp$ is independent of K ; it is not affected by longitudinal gradients [20]. The outward Cartesian radius parameter R_o reflects the effective lifetime of the source (in the frame in which the expressions on the r.h.s. are evaluated) via [12, 47]

$$R_{\text{diff}}^2 \equiv R_o^2 - R_s^2 = \beta_\perp^2 \langle \tilde{t}^2 \rangle + 2\beta_\perp \langle \tilde{x}\tilde{t} \rangle + \langle \tilde{x}^2 - \tilde{y}^2 \rangle. \quad (26)$$

Due to the absence of transverse flow the last two terms vanish here. The effective lifetime in the YK frame (i.e. in the rest frame of the effective source) is measured by R_0 in the YKP parametrization [19, 20]. Due to different kinematic factors the lifetime effects are stronger and more easily visible in R_0 than in R_o . Fig. 2 also confirms the observation [12, 19] that the M_\perp dependence of the effective emission duration is connected with the M_\perp dependence of the longitudinal region of homogeneity which results from longitudinal expansion [9].

The decrease of R_{\parallel} near the edge of the rapidity distribution results from an interplay between the Gaussian space-time rapidity distribution and the Boltzmann factor in the emission function. It gives rise to a narrowing rapidity width of the effective source with increasing pair rapidity Y_{CM} . At large M_{\perp} , the longitudinal radii R_l and R_{\parallel} are independent of the pair rapidity Y_{CM} , due to the longitudinal boost-invariance of the velocity profile in the Boltzmann factor which dominates the shape of the emission function in the limit $M_{\perp} \rightarrow \infty$.

It is interesting to compare the longitudinal Cartesian radius parameter R_l in the LCMS frame with the longitudinal YKP radius R_{\parallel} . For small M_{\perp} , R_l is larger than R_{\parallel} , although not by much, while at large M_{\perp} the two parameters agree. This can be understood by recalling the relation [19]

$$R_l^2 = (1 - \beta_l)^2 R_{\parallel}^2 + \gamma^2 (\beta_l - v)^2 (R_0^2 + R_{\parallel}^2) \quad (27)$$

which, together with two other such relations [19], expresses the mathematical equivalence of the Cartesian and YKP parametrizations. For large M_{\perp} the source velocity v coincides with the longitudinal velocity β_l of the pair (which is zero in the LCMS). Then the second term in (27) vanishes and $R_l^2 = R_{\parallel}^2$ in the LCMS. For smaller values of M_{\perp} and $Y_{\text{CM}} \neq 0$ the pair and source velocities β_l and v are slightly different [19]; the resulting positive contribution from the second term in (27) renders $R_l^2 > R_{\parallel}^2$ unless R_0^2 turns negative (see Sec. 5). This feature was already observed by Podgoretskii [33] who introduced the Yano-Koonin frame as the frame in which the production process is reflection symmetric with respect to the longitudinal direction. Within a class of non-expanding models he showed that in this frame the longitudinal source radius is minimal. On first sight this appears to contradict the laws of special relativity from which one might expect that the longitudinal homogeneity length of the source should be *largest* in the source rest frame and appear Lorentz *contracted* in any other frame. This argument neglects, however, the fact that different points of the homogeneity region generally freeze out at different times⁵ (see Figs. 2c,d).

The cross term R_{ol}^2 shown in the lower right panel of Fig. 3 is required by the invariance of the correlation function under longitudinal boosts of the measurement frame [10, 11]. Its value and M_{\perp} dependence depends strongly on the measurement frame; for example, in the CMS the cross term is negative with smaller absolute value [49] although its generic M_{\perp} dependence remains similar.

Except for R_o and R_{ol}^2 , all radius parameters shown in Fig. 3 scale with the transverse mass M_{\perp} and show no explicit dependence on the particle rest mass. The curves for pions and kaons thus coincide. This scaling is broken for R_o and R_{ol}^2 by the appearance of explicit factors β_{\perp} in Eqs. (4) and (6). A quantitative measure for the strength of the M_{\perp} dependence can be obtained by fitting the radius to a power law, $R_i(M_{\perp}) \propto M_{\perp}^{-\alpha_i}$, $i = l, \parallel, 0$ [26, 27]. The corresponding exponents are listed in Table 2. The longitudinal radius parameters R_l and R_{\parallel} scale approximately with $1/\sqrt{M_{\perp}}$ as predicted in Ref. [9]. The scaling power is generally closer to -0.5 for kaons than for pions; this is due to their larger rest mass which reflects in larger values for M_{\perp} where the saddle point approximation and the assumption of longitudinal boost-invariance in Ref. [9] become better. For the temporal YKP parameter R_0 the $1/\sqrt{M_{\perp}}$ scaling law does not hold – it decreases more slowly, especially at larger M_{\perp} and for kaons.

⁵We thank Ján Pišút for a clarifying discussion on this point.

Table 2: The exponents found by a fit of the HBT radii with the function $R_i(M_\perp) \propto M_\perp^{-\alpha_i}$, $i = l, \parallel, 0$, for a transparent source without transverse expansion and temperature gradients.

		Y_{CM}		
		0	1.5	3
α_l	pions	0.568	0.585	0.626
	kaons	0.546	0.553	0.573
α_\parallel	pions	0.568	0.542	0.478
	kaons	0.546	0.538	0.515
α_0	pions	0.403	0.380	0.321
	kaons	0.202	0.197	0.185

4.2 Effects from individual types of gradients

In this subsection we investigate separately the effects of specific types of gradients in the emission function on the two-particle correlations, discussing at the same time the corresponding single particle spectra. A simultaneous analysis of one- and two-particle spectra is required for a clear separation of thermal and collective features of the source and for a complete reconstruction of its emission function [14, 50, 51].

We begin with the discussion of gradient effects on the single particle spectra. Fig. 4 shows the influence of transverse and temporal temperature gradients and of transverse

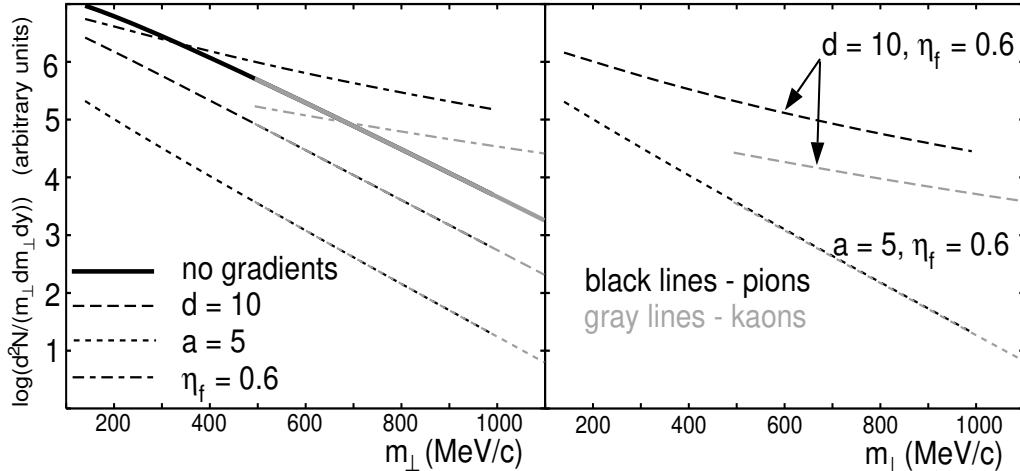


Figure 4: Transverse mass spectra at midrapidity from a transparent source. Black lines correspond to pions, gray lines to kaons. In the left plot the effects from different types of gradients are shown individually, in the right plot we study the interplay of transverse temperature gradients with transverse flow.

flow on the m_\perp -spectra at fixed $Y_{\text{CM}} = 0$. Qualitatively very similar features are seen

at other rapidity values and in the rapidity integrated spectra. One sees that even very strong temporal and transverse temperature gradients do not cause any major effects on the single particle spectra, compared to the case without any gradients. Their main effect is a change of the normalization because the colder regions of the emission function contribute less; their contribution is also concentrated at smaller momenta, leading to a somewhat steeper slope of the transverse mass spectra at low m_\perp .

This situation changes dramatically when the source develops transverse collective flow. In the absence of temperature gradients, transverse flow simply flattens the m_\perp -spectra [52]. For large $m_\perp \gg m_0$ (i.e. relativistic momenta) this can be described in terms of an effective blueshifted temperature $T_{\text{eff}} = T \sqrt{\frac{1+\langle v(r) \rangle}{1-\langle v(r) \rangle}}$ which is the same for all particle species while at small m_\perp the flattening is even stronger and depends on the particle mass via the nonrelativistic relation $T_{\text{eff}} = T + m \langle v(r) \rangle^2$ [52]. These features have now been clearly observed in the heavy collision systems studied at the Brookhaven AGS and CERN SPS [53]. Transverse flow clearly also breaks the m_\perp scaling between pions and kaons: the pion and kaon spectra in the left panel of Fig. 4 have different slopes and normalizations.

Additional temperature gradients which are imposed on top of the transverse expansion flow affect the spectra as shown in the right panel of Fig. 4. A temporal gradient of the source temperature has no qualitative effect on the shape of the m_\perp spectra and only affects their normalization. A transverse spatial gradient of the temperature, however, interferes seriously with the transverse flow by strongly reducing its effect on the slope of the m_\perp spectra. For a strong transverse temperature gradient with $a = 5$ as shown in the Figure, a comparison with the left panel shows that the flow effects become nearly invisible. An analytical discussion of this behaviour is given in [14] where it is shown to occur if the transverse homogeneity length generated by temperature gradient becomes much smaller than the one generated by the transverse velocity gradient. It follows from this discussion that it is not possible to generate a strong (additional) M_\perp -dependence of the transverse HBT radius parameter from transverse temperature gradients (see below) without at the same time reducing the flow effects on the single particle m_\perp spectra.

We now proceed to a discussion of the HBT radius parameters. The effect of temporal temperature gradients is studied in Fig. 5. As expected, they affect mostly those HBT parameters which are sensitive to the effective lifetime of the source, namely the temporal YKP parameter R_0 and the Cartesian difference $R_o^2 - R_s^2$. These are reduced by increasing d . The origin of this effect can be seen in Fig. 2 which shows that larger values of d concentrate the high temperature region (with large emissivity) to a narrower region in the z - t plane. The narrowing occurs predominantly in the temporal direction, but affects slightly also the longitudinal homogeneity length. Going from central rapidity to pairs at forward rapidities, all curves change in a similar way as shown in Fig. 3.

Transverse temperature gradients leave their traces only in the transverse homogeneity length measured by $R_s = R_\perp$. In Fig. 6 this is shown for pions and kaons at mid-rapidity. (Note that in our model R_s is rapidity independent.)

The most important feature of both types of temperature gradients is that they *do not break the M_\perp scaling of the YKP correlation radii* found in previous subsection. Note also that the temperature gradients have no qualitative impact on the YK rapidity

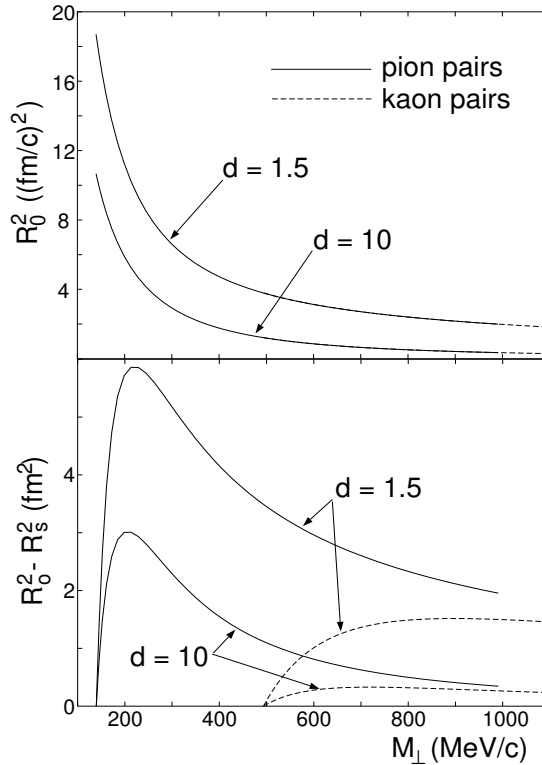


Figure 5: The effects of temporal temperature gradients on the temporal YKP parameter R_0 (upper panel) and the difference $R_o^2 - R_s^2$ in the Cartesian parametrization (lower panel). Solid (dashed) lines are for pions (kaons). The calculations are done for midrapidity pairs, $Y_{\text{CM}} = 0$, and for $a = \eta_f = 0$, $\lambda = \infty$.

Y_{YK} associated with the YK velocity v .

Many of these features change in the presence of transverse flow. This is shown in Fig. 7 for pairs with rapidity $Y_{\text{CM}} = 1.5$ in the CMS. All radius parameters have been calculated from space-time variances evaluated in the LCMS. The choice of a non-zero CMS pair rapidity ensures a non-vanishing cross term R_{ol} . The generic rapidity dependence of the radii follows the behaviour discussed in Sec. 4.1.

Since transverse flow introduces velocity gradients in the transverse direction, $R_s (= R_\perp)$ and R_o decrease with increasing η_f . Less obvious is, however, the rather strong effect of transverse flow on the “temporal” YKP parameter R_0^2 . For higher transverse masses the latter even begins to increase with M_\perp . This does not, however, reflect the behaviour of the emission duration which continues to decrease for particles with higher M_\perp . The increase of R_0^2 is rather caused by correction terms expressing the difference between R_0^2 and the lifetime [19, 20]:

$$R_0^2 - \langle \tilde{t}^2 \rangle = \frac{2}{\beta_\perp} \langle \tilde{x} \tilde{t} \rangle + \frac{1}{\beta_\perp^2} \langle \tilde{x}^2 - \tilde{y}^2 \rangle. \quad (28)$$

Especially the second term on the r.h.s. grows appreciably with increasing η_f , and

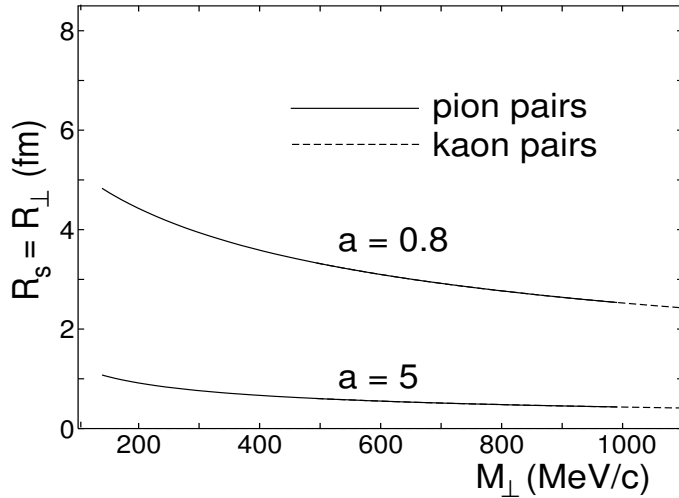


Figure 6: The effect of a transverse temperature gradient: The transverse radius parameter $R_s = R_\perp$ as a function of the transverse mass of the pair, for two different values of a . The coincidence of the solid (dashed) lines for pions (kaons) reflects the M_\perp -scaling of the transverse radius in this case. $d = \eta_f = 0$, $\lambda = \infty$, $Y_{\text{CM}} = 0$.

even more so for pions than for kaons. This was studied in detail in Ref. [20] (cf. Fig. 2 of that paper) where a more detailed explanation of the curves for R_0^2 shown here can be found.

The most important feature of Fig. 7 is the *breaking of the M_\perp scaling of the YKP radii by the transverse flow*.

4.3 Interplay of all gradients

In Ref. [14] it was claimed that an interplay of the various types of gradients discussed above can lead to a common $1/\sqrt{M_\perp}$ scaling law for all three Cartesian HBT radii, R_ℓ , R_s , and R_o , as well as for the effective lifetime of the source. The condition for such a common scaling is that the geometric extension is large compared to the “thermal length scales” generated by temperature and flow gradients [14]. The claim of Ref. [14] was based on approximate analytical expressions for these radius parameters which were obtained by evaluating the corresponding integrals over the emission function within an improved saddle-point approximation scheme. In this subsection we present a numerical test of this claim. To this end we select a set of parameters ($a = 0.6$, $d = 10$, $\eta_f = 0.25$) for which at mid-rapidity the conditions for such a scaling, as given in Ref. [14], are satisfied as much as possible, without leaving the phenomenologically realistic range.

The numerically evaluated correlation radii for this parameter set are plotted with thick lines in Fig. 8. The analytical approximation according to Ref. [14] is shown by the thin lines for comparison. We agree with the conclusions drawn from a similar comparison presented in Ref. [22] that for kaons the approximate analytical formulae

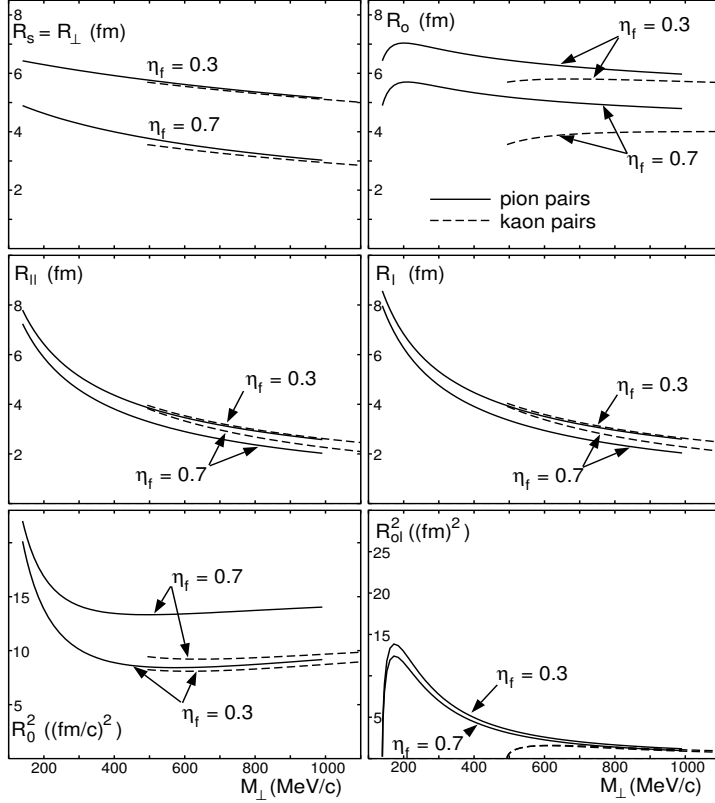


Figure 7: The correlation radii for a transparent source of constant temperature featuring transverse collective flow. The rapidity of the pairs was chosen as $Y_{\text{CM}} = 1.5$. Left column: YKP radius parameters. Right column: Cartesian radius parameters. Solid (dashed) lines correspond to pions (kaons).

agree with the numerical curves within 15%. For pions with transverse momenta below 600 MeV the discrepancies are larger because one of the conditions of validity of the analytical formulae (sufficiently large M_{\perp}) is violated. However, the analytical approximation does not give at all the (slight) breaking of the M_{\perp} scaling of R_l by the transverse flow, and at mid-rapidity it misses the initial rise of R_o at small M_{\perp} . This last point in particular is a serious problem if one wishes to extract an estimate of the effective lifetime according to Eq. (26). Similar (dis-)agreement at a comparative level is seen for forward rapidity pairs at $Y_{\text{CM}} = 1.5$, with the exception of the cross term R_{ol} which is strongly overestimated by the approximation. The analytical approximation of Ref. [14] is restricted by the condition that the flow rapidity of the point of maximum emissivity in the LCMS is small. Since the latter coincides with good approximation with the YK rapidity [19] and, in our model, the YK rapidity is found to converge to Y in the limit $M_{\perp} \rightarrow \infty$ [19, 20], the point of maximum emissivity moves to zero LCMS rapidity in that limit. This explains why for large M_{\perp} the analytical and numerical results agree.

On a superficial level the analytical approximations of Ref. [14] thus don't seem to

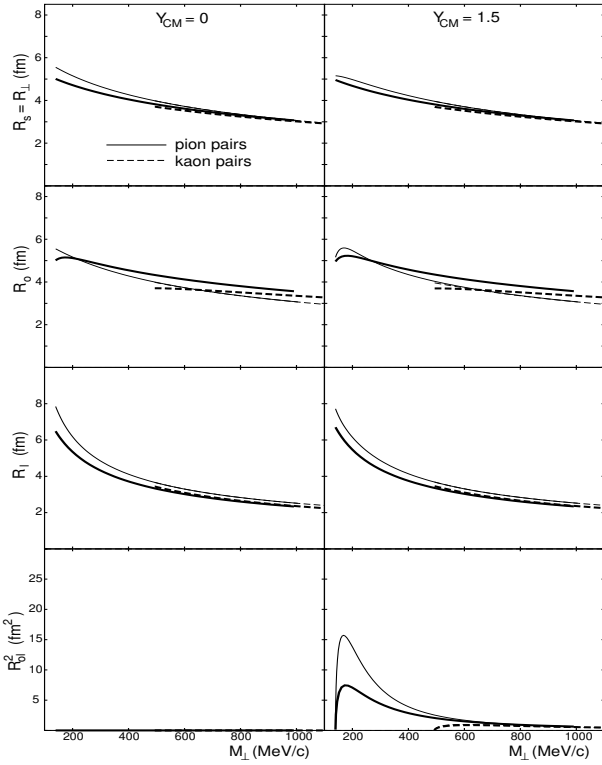


Figure 8: Correlation radii in the Cartesian parametrization for a transparent source with parameters $a = 0.6$, $d = 10$, $\eta_f = 0.25$, $\lambda = \infty$. The thick lines represent the exact result from a numerical evaluation of the space-time variances, the thin lines use the approximate analytical formulae given in [14]. Solid (dashed) lines are for pions (kaons).

be doing too badly. We want to check, however, whether the results also confirm the suggested $1/\sqrt{M_\perp}$ -scaling. In Ref. [20] it was shown that in general the strength of the M_\perp -dependence of R_s and R_l (resp. R_\perp and R_{\parallel}) is correlated with the strength of collective flow in the transverse resp. longitudinal directions. One way of quantifying the strength of the M_\perp -dependence of the correlation radii is to fit them to a power law $R_i \propto M_\perp^{-\alpha_i}$ ($i = s, l, \parallel, 0$) and to study the values of the exponents α_i . According to the approximate formulae of Ref. [14], at mid-rapidity all these powers should be equal to 0.5. The α_i -values obtained from the numerically evaluated correlation radii are listed in Table 3. One sees that only the longitudinal radius parameters (both in YKP and Cartesian parametrizations) follow an approximate $1/\sqrt{M_\perp}$ scaling law, similar to previous studies without temperature gradients [12, 20]. It reflects the boost-invariance of the longitudinal expansion velocity profile [9]. The transverse and temporal radius parameters $R_s = R_\perp$ and R_0 scale much more weakly with M_\perp . For mid-rapidity kaons R_0 provides a good estimate for the emission duration because for $\eta_f = 0.25$ the correction terms on the r.h.s. of (28) are small; thus we find that also the effective lifetime of the source does not scale with $1/\sqrt{M_\perp}$. Thus, while the conditions for

Table 3: The exponents α_i found in a fit of the numerically computed correlation radii to a power law $R_i \propto M_{\perp}^{-\alpha_i}$, for a source with the parameters given in Fig. 8

		Y_{CM}		
		0	1.5	3
α_s	pions	0.253	0.249	0.236
	kaons	0.294	0.291	0.285
α_l	pions	0.519	0.534	0.572
	kaons	0.534	0.539	0.552
α_{\parallel}	pions	0.519	0.503	0.458
	kaons	0.534	0.527	0.506
α_0	pions	0.282	0.270	0.238
	kaons	0.108	0.106	0.102

the saddle point approximation in Ref. [14] are satisfied with sufficient accuracy by our (semi-realistic) parameter set, the stronger conditions required for the common $1/\sqrt{M_{\perp}}$ -scaling are not.

5 One- and two-particle spectra from opaque sources

In this Section we focus our attention on opaque sources. We look for specific signals for opacity in a simultaneous analysis of one- and two-particle spectra. We will show that opacity leads to dramatic effects in the YKP parameter R_0^2 which can be exploited experimentally.

5.1 One-particle spectra

In Fig. 9 we compare the single particle m_{\perp} -spectra from transparent and opaque source with and without transverse flow. For non-expanding sources, the slopes are identical for opaque and transparent sources; the normalization is reduced in the opaque source because effectively a much smaller region contributes to particle emission. For expanding sources with a fixed value of η_f , the spectrum from the opaque source is much flatter than from the corresponding transparent source: due to the opacity, much stronger weight is given to the rapidly expanding surface than to the less rapidly expanding interior regions. Correspondingly, the *average* flow velocity is larger for the opaque source, leading to a larger “effective temperature” T_{eff} (see discussion after Fig. 4). As seen in Fig. 9 (thick dash-dotted line), a similar slope for the spectrum from the opaque source can be obtained by reducing the transverse flow⁶ in the opaque source from $\eta_f = 0.6$ to $\eta_f = 0.25$. For this value the average transverse expansion velocity in the opaque source,

$$\langle v_{\perp} \rangle = \frac{1}{N} \int_0^{\infty} r dr \int_0^{2\pi} d\phi v_{\perp}(r) \exp\left(-\frac{r^2}{2R^2}\right) \exp\left(-\kappa \frac{l_{\text{eff}}(r, \phi)}{\lambda}\right) \quad (29)$$

⁶The size of this source was also scaled (see following subsection) but in the single particle spectrum this affects only the normalization.

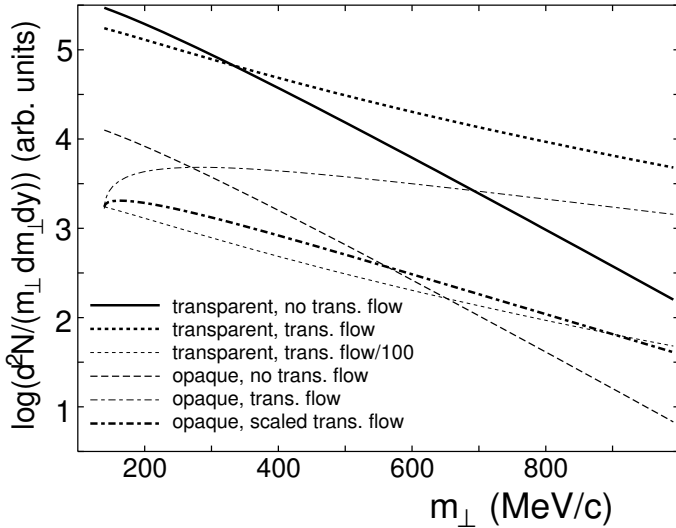


Figure 9: Comparison of m_{\perp} -spectra for transparent and opaque sources at mid-rapidity. For the model parameters see Table 1. The thick solid line for a transparent source without flow is shown for reference. The thick dotted line shows the effect of adding transverse flow with $\eta_f = 0.6$, the thin dotted line is the same spectrum divided by a factor 100. The dashed line shows the spectrum from an opaque source with $\lambda = R/14 = 0.5$ fm in the absence of transverse flow. The dash-dotted lines show spectra from expanding opaque sources: the thin line corresponds to $\eta_f = 0.6$, the thick line to $\eta_f = 0.25$ in a scaled source with $R = 3.129$ fm and $\lambda = R/14 = 0.223$ fm (see text for discussion).

$$\begin{aligned}
&= \frac{1}{N} \int_0^\infty r dr \left[\tanh \left(\eta_f \frac{r}{R} \right) \exp \left(-\frac{r^2}{2R^2} \right) \right. \\
&\quad \times \left. \int_0^{2\pi} d\phi \exp \left(-\frac{\kappa}{\lambda} e^{-\frac{r^2 \sin^2 \phi}{2R^2}} \int_{r \cos \phi}^\infty e^{-\frac{x^2}{2R^2}} dx \right) \right], \\
N &= \int_0^\infty r dr \left[\exp \left(-\frac{r^2}{2R^2} \right) \int_0^{2\pi} d\phi \exp \left(-\frac{\kappa}{\lambda} e^{-\frac{r^2 \sin^2 \phi}{2R^2}} \int_{r \cos \phi}^\infty e^{-\frac{x^2}{2R^2}} dx \right) \right],
\end{aligned}$$

agrees with the average transverse expansion velocity of a transparent source with $\eta_f = 0.6$. One notes, however, that in spite of the similar slopes arranged by this procedure, the shapes of the spectra still differ in detail. In particular, the spectrum from the opaque source features a clear ‘‘shoulder’’ at small p_{\perp} , resembling the ‘‘blast wave’’ picture of Ref. [54]. This is due to the strong weighting of a single value of the transverse velocity by the opaque source with its sharply peaked surface emission pattern. Presently available single particle spectra [53] do not seem to support the existence of such a blast-wave peak at small, but non-zero p_{\perp} which should be even more pronounced for heavier particles [54].

5.2 Correlation radii

As for the single particle spectra, we restrict our discussion of the correlation radii from opaque sources to the effects from transverse flow, neglecting temperature gradients. In this case, for midrapidity pairs ($Y_{\text{CM}} = 0$) the cross term R_{ol} vanishes, and $R_l = R_{\parallel}$. The remaining four radius parameters $R_s = R_{\perp}$, R_o , R_0 , and $R_l = R_{\parallel}$, are shown in Fig. 10. Surprisingly, in the absence of transverse flow the outward radius decreases

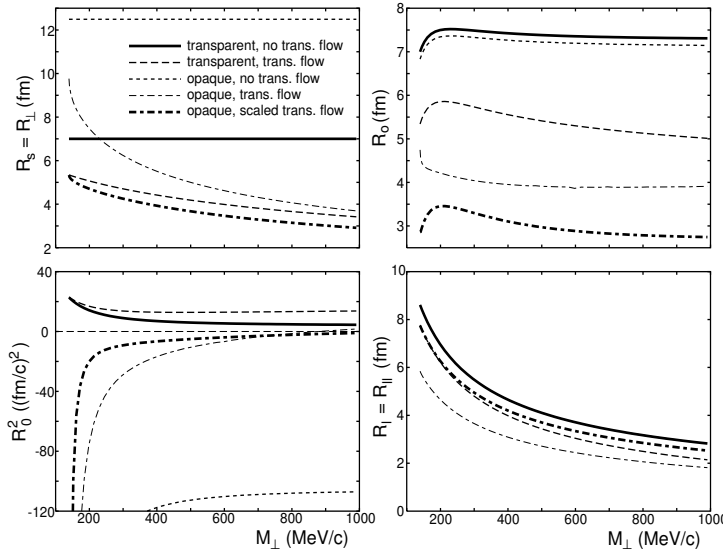


Figure 10: Correlation radii from transparent and opaque sources with constant temperature, for pion pairs with rapidity $Y_{\text{CM}} = 0$. The source parameters are given in Table 1. Solid (dashed) lines: transparent source with $\eta_f = 0$ ($\eta_f = 0.6$). Dotted lines: opaque source ($\lambda = 0.5$ fm = $R/14$) without transverse flow ($\eta_f = 0$). (For R_l this line coincides with the solid line.) Dash-dotted lines: opaque source with transverse flow (thin: $R = 7$ fm, $\lambda = 0.5$ fm, $\eta_f = 0.6$; thick: $R = 3.129$ fm, $\lambda = 0.223$ fm, $\eta_f = 0.25$). For the thick dash-dotted lines the scaled parameters were chosen such that the average transverse flow velocity and the transverse HBT radius R_s at $K_{\perp} = 0$ agree with that of the expanding transparent source (dashed lines).

only weakly when going from transparent source to the opaque one. On the other hand, the sideward radius increases dramatically. Fig. 1 provides the explanation for this somewhat unexpected behaviour: due to the exponential suppression resulting from the “opacity factor” $\exp(-\kappa l_{\text{eff}}/\lambda)$ in (20), the dense interior of the cylinder with radius R is essentially cut out from the emission function, and the effective source becomes part of a thick shell with a radius $R_{\text{shell}} > R$. The large shell radius results in a large sideways homogeneity radius R_s . The value of R_o at $K_{\perp} = 0$, given by the extension of the emitting half-shell in outward direction, is accidentally close to the outward radius for the transparent source. Note that this feature of an apparently larger effective source in the case of opaqueness is a consequence of our Gaussian transverse density profile which allows the emission region to “expand” into the dilute

tail of the distribution when the dense interior is eliminated by opacity effects. Such a possibility does not exist in the model investigated by Heiselberg and Vischer [17, 18] who use a box profile for the density distribution. In this case no emission from regions outside the box radius R is possible, and opacity instead leads to an effective emission function which is “squeezed” into a very thin crescent-shaped region close to the edge of the box.

For transparent sources it is well known that transverse flow causes a reduction of the sideward and outward homogeneity regions $\langle \tilde{y}^2 \rangle$ and $\langle \tilde{x}^2 \rangle$, respectively, the more so the larger M_\perp [11, 12, 13, 14]. For fixed transverse flow parameter η_f , this effect is seen to be even stronger for opaque sources, in both absolute and relative terms. This can be understood by remembering from the preceding subsection that, for fixed η_f , the average transverse flow velocity is considerably larger in the opaque than in the transparent source. For the outward radius this effect even eliminates the weak rise of R_o for small K_\perp (cf. the thin dash-dotted line in the right upper panel of Fig. 10). This implies that the decrease of $\langle \tilde{x}^2 \rangle$ with transverse mass is stronger than the increasing contribution from $\beta_\perp^2 \langle \tilde{t}^2 \rangle$. (The relative magnitudes of the various contributions to R_o is shown in the lower left panel of Fig. 11, although for a smaller value of η_f .)

It is obvious from Fig. 10 that for given experimental values for R_s the opaque source must be scaled down in R relative to a transparent source. The thick dash-dotted lines in Fig. 10 show the HBT radii for such a “scaled opaque source” in which η_f is reduced to give the same average transverse expansion velocity as $\eta_f = 0.6$ in a transparent source, and R is rescaled such that $R_s(M_\perp = m_\pi)$ from both models agrees. To keep the same degree of opacity, also λ is reduced keeping the ratio $\lambda/R = 1/14$ fixed. After this rescaling, the opaque and transparent sources exhibit rather similar sideward radii $R_s(m_\perp)$. However, the outward radius of the opaque source is still much smaller than the one of the corresponding transparent source, even if the rise at small values of K_\perp has reappeared. As seen in Fig. 11, the reason is that for the opaque source $\langle \tilde{x}^2 \rangle \ll \langle \tilde{y}^2 \rangle$.

This effect is dramatically enhanced in the parameter R_0^2 of the YKP parametrization which is given by Eq. (28). For opaque sources the second term on the r.h.s. is negative and diverges to $-\infty$ as $K_\perp \rightarrow 0$ ($\beta_\perp \rightarrow 0$). Transverse flow reduces this negative contribution, but not sufficiently to reverse the overall negative sign of R_0^2 in the region of small K_\perp . As we will see in the following subsection, this specific feature of opaque sources is quite stable against a reduction of the opacity of the source in the sense that it even shows up for nearly transparent sources with $\lambda \sim R$.

Compared to R_s , R_o , and R_0 , the opacity effects on $R_l = R_{\parallel}$ (shown in the lower right panel of Fig. 10) are weak. They can all be explained in terms of the different values for the average transverse flow velocities in the studied examples (cf. Fig. 7).

The interesting opacity effects on $R_o^2 - R_s^2$ and on R_0^2 deserve a more detailed discussion. To this end we plot in Fig. 11 the various contributions to these radius parameters from the space-time variances of a transparent (upper row) and an opaque source (lower row), both for the standard Cartesian (left column) and YKP parametrizations (right column). We show results for moderate transverse flow $\eta_f = 0.3$ and midrapidity pion pairs, but we checked that no qualitative differences occur for forward rapidities. The diagrams in Fig. 11 can be concisely summarized by stating that for transparent sources the lifetime term $\langle \tilde{t}^2 \rangle$ dominates the difference $R_o^2 - R_s^2$ and R_0^2 (at least for small K_\perp) while for opaque sources the difference $\langle \tilde{x}^2 - \tilde{y}^2 \rangle$ of transverse spatial variances takes

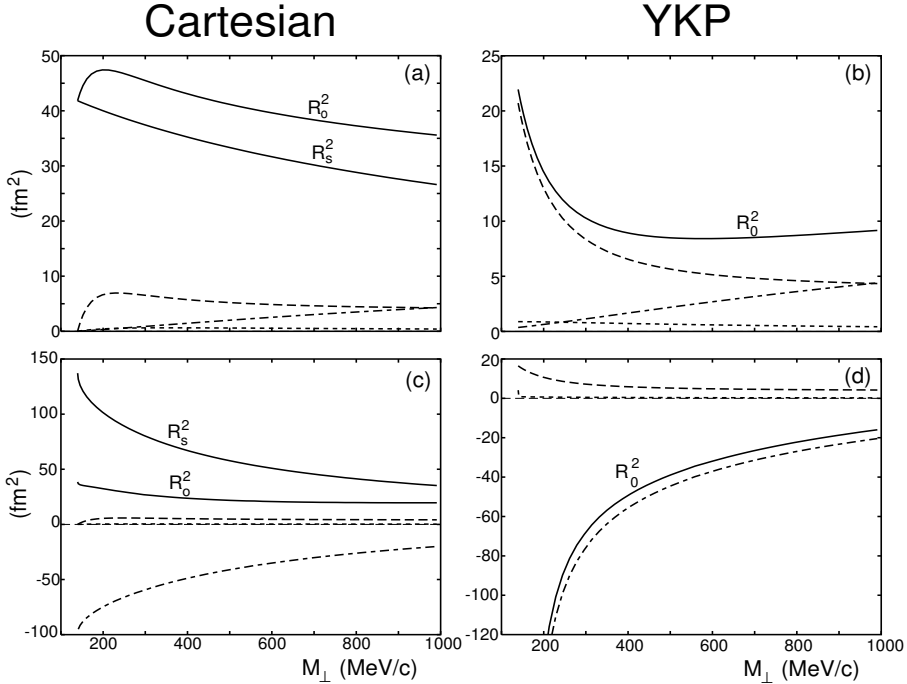


Figure 11: Opacity effects on $R_o^2 - R_s^2$ (left column) and R_0^2 (right column). The solid lines show the radius parameters as they enter the correlation function, the other lines show how they are decomposed into contributions from various space-time variances. Left column: the dashed line shows $\beta_{\perp}^2 \langle \tilde{t}^2 \rangle$, the dotted line $-2\beta_{\perp} \langle \tilde{x}\tilde{t} \rangle$, and the dash-dotted line $\langle \tilde{x}^2 - \tilde{y}^2 \rangle$. In the right column the same symbols denote the same quantities divided by β_{\perp}^2 . All curves are calculated at $Y_{\text{CM}} = 0$, with model parameters from Table 1 and $\eta_f = 0.3$. Upper row: $\lambda = \infty$ (transparent source); lower row: $\lambda = 0.5 \text{ fm}$ (opaque source).

the leading role.

These results confirm the conclusion of Ref. [17] that, within the Cartesian parametrization, opaque sources generically lead to negative values for the difference $R_o^2 - R_s^2$. Our calculations were done in the YK frame, and we checked that in this frame this qualitative conclusion is independent of the pair rapidity. In the YKP parametrization the same feature appears strongly enhanced in the parameter R_0^2 , especially at small values of K_{\perp} , due to the division of the relevant combination of space-time variances by the factor β_{\perp}^2 . A negative value for R_0^2 corresponds to a negative value for $R_o^2 - R_s^2$ in the YK frame (which is usually not much different from the LCMS [20]).

In Fig. 12 we investigate the stability of this feature against variations in the amount of transverse flow and the opacity of the source. For sources without transverse flow ($\eta_f = 0$) R_0^2 is seen to stay negative for all values of M_{\perp} even for nearly transparent sources with $\lambda = 2R$. Once transverse flow is switched on, the flow-induced reduction of both transverse homogeneity lengths $\sqrt{\langle \tilde{x}^2 \rangle}$ and $\sqrt{\langle \tilde{y}^2 \rangle}$ causes R_0^2 to turn positive at sufficiently large values of M_{\perp} ; a region of strongly negative R_0^2 values survives,

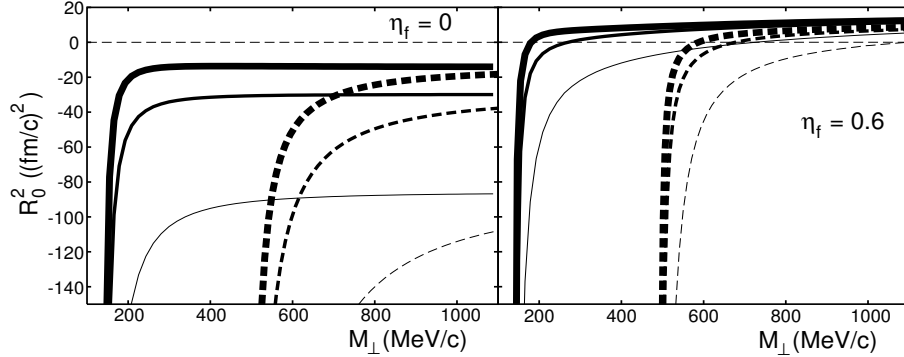


Figure 12: The YKP parameter $R_0^2(M_\perp)$ for midrapidity pairs for various combinations of λ and η_f (no temperature gradients, source parameters from Table 1). Solid (dashed) lines are for pions (kaons). Thin lines: $\lambda = 1 \text{ fm} = R/7$; medium lines: $\lambda = 7 \text{ fm} = R$; thick lines: $\lambda = 14 \text{ fm} = 2R$. Left diagram: $\eta_f = 0$; right diagram: $\eta_f = 0.6$.

however, at small M_\perp . This region is larger for sources with strong opacity (small λ) than for more transparent ones, but even for $\lambda = 2R$ it does not disappear completely.

The preliminary 158 GeV/c Pb+Pb data from the NA49 Collaboration at CERN [28, 29, 30] show positive values for R_0^2 in all pair rapidity bins Y and for all values of M_\perp . The lowest M_\perp bin corresponds to transverse pair momenta below 100 MeV/c. Of course, the curves shown in Fig. 12 depend to some extent on the transverse density profile of our model source. Still, by not seeing any signs for negative values of R_0^2 , it appears that the NA49 data eliminate the possibility that the source is strongly surface dominated ($\lambda \ll R$) and favor an emission function where particles moving in a given direction \mathbf{K} are emitted more or less from the whole fireball volume.

5.3 Modified YKP parametrization

In this subsection we point out and repair a deficiency of the YKP parametrization which went so far unnoticed but can become important particularly for opaque sources.

In Fig. 13 we show the YKP radius parameters R_0^2 and R_{\parallel} as well as the YK rapidity $Y_{\text{YK}} = 0.5 \ln[(1+v)/(1-v)]$ (relative to the LCMS) for pion pairs at forward rapidity $Y_{\text{CM}} = 1.5$ for transparent and opaque sources with and without transverse flow. Let us first look at the Yano-Koonin rapidity Y_{YK} : For transparent sources we reproduce the known feature [19, 20] that the YK rapidity is negative in the LCMS, i.e. that the effective source moves somewhat more slowly in the beam direction than the emitted pairs. For opaque sources the opposite seems to be the case: at least for pairs with small transverse masses, the YK rapidity is positive in the LCMS. It is important to point out that this does *not* imply that in this case the effective source moves faster than the emitted pairs (which would be counterintuitive); it rather reflects the fact that for opaque sources the geometric correction terms in the expression for the YK velocity (see Eq. (4.1) in Ref. [20]), in particular the one proportional to $\langle \tilde{x}^2 - \tilde{y}^2 \rangle$, are large and spoil the interpretation of v as the longitudinal source velocity.

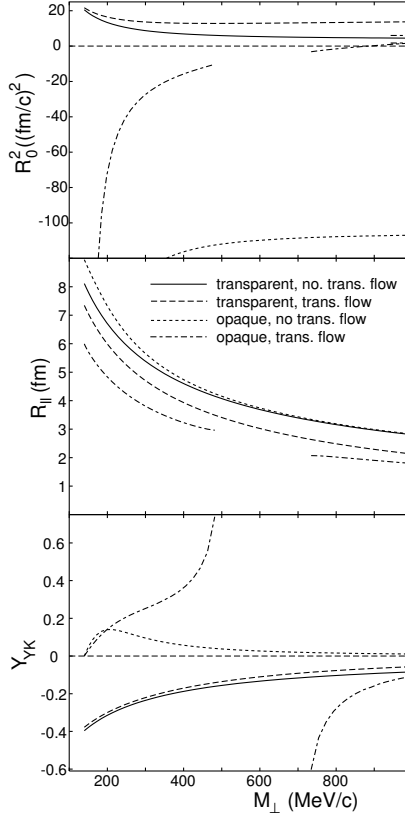


Figure 13: YKP radii and YK rapidity in the LCMS for pion pairs at $Y_{\text{CM}} = 1.5$. Solid and dashed lines represent the results for a transparent source with $\eta_f = 0$ and $\eta_f = 0.6$, respectively. The radii for an opaque source with $\lambda = R/14 = 0.5$ fm are shown as dotted ($\eta_f = 0$) and dot-dashed lines ($\eta_f = 0.6$), respectively. The gap in the dot-dashed curves corresponds to a region where the YKP parametrization is not defined. (No temperature gradients.)

As seen in the dot-dashed curves for an expanding opaque source, these correction terms can cause even more severe problems: the curves feature a gap, inside which the argument of the square root in Eq. (14) turns negative and the YK velocity (and thus also R_0^2 and R_{\parallel}^2 , see Eqs. (15), (16)) become undefined. The conditions for the occurrence of such a pathological behaviour are discussed in Appendix A. It appears that it is connected in a generic way to $\langle \tilde{x}^2 \rangle < \langle \tilde{y}^2 \rangle$ which, as we have seen, characterizes opaque sources.

This problem with the YKP parametrization can be avoided by a simple technical modification which we call ‘‘Modified Yano-Koonin-Podgoretskii’’ parametrization. It differs from the YKP parametrization by using q_s rather than $q_{\perp} = \sqrt{q_s^2 + q_o^2}$ as one of the three independent components of the relative momentum q . For distinction we denote the corresponding HBT parameters with a prime:

$$C(\mathbf{q}, \mathbf{K}) = 1 + \exp \left[-R_{\perp}'^2(\mathbf{K}) q_s^2 - R_{\parallel}'^2(\mathbf{K}) (q_l^2 - (q^0)^2) \right] \quad (30)$$

$$- \left(R_0'^2(\mathbf{K}) + R_{\parallel}'^2(\mathbf{K}) \right) (q \cdot U'(\mathbf{K}))^2 \right]$$

with

$$U'(\mathbf{K}) = \gamma'(\mathbf{K})(1, 0, 0, v'(\mathbf{K})). \quad (31)$$

Introducing in analogy to (11)-(13) the shorthands

$$A' = \langle \tilde{t}^2 \rangle - \frac{2}{\beta_{\perp}} \langle \tilde{t} \tilde{x} \rangle + \frac{1}{\beta_{\perp}^2} \langle \tilde{x}^2 \rangle, \quad (32)$$

$$B' = \langle \tilde{z}^2 \rangle - 2 \frac{\beta_l}{\beta_{\perp}} \langle \tilde{z} \tilde{x} \rangle + \frac{\beta_l^2}{\beta_{\perp}^2} \langle \tilde{x}^2 \rangle, \quad (33)$$

$$C' = \langle \tilde{z} \tilde{t} \rangle - \frac{\beta_l}{\beta_{\perp}} \langle \tilde{t} \tilde{x} \rangle - \frac{1}{\beta_{\perp}} \langle \tilde{z} \tilde{x} \rangle + \frac{\beta_l}{\beta_{\perp}^2} \langle \tilde{x}^2 \rangle, \quad (34)$$

the modified HBT parameters can be expressed by the same formulae as the original YKP parameters:

$$v' = \frac{A' + B'}{2C'} \left(1 - \sqrt{1 - \left(\frac{2C'}{A' + B'} \right)^2} \right), \quad (35)$$

$$R_{\parallel}'^2 = B' - v' C', \quad (36)$$

$$R_0'^2 = A' - v' C', \quad (37)$$

$$R_{\perp}'^2 = \langle \tilde{y}^2 \rangle. \quad (38)$$

In the modified YK frame, defined by $v' = 0$, we thus have $R_{\parallel}'^2 = B'$ and $R_0'^2 = A'$. Of course, since both YKP and Modified YKP parametrisations are just two ways of parametrizing the same correlation function, they are related in a simple way:

$$A = \gamma'^2 R_0'^2 + \gamma'^2 v'^2 R_{\parallel}'^2 - \frac{1}{\beta_{\perp}^2} R_{\perp}'^2, \quad (39)$$

$$B = \gamma'^2 R_{\parallel}'^2 + \gamma'^2 v'^2 R_0'^2 - \frac{\beta_l^2}{\beta_{\perp}^2} R_{\perp}'^2, \quad (40)$$

$$C = (R_0'^2 + R_{\parallel}'^2) \gamma'^2 v' - \frac{\beta_l}{\beta_{\perp}^2} R_{\perp}'^2. \quad (41)$$

The inverse relations are given by

$$A' = \gamma^2 R_0^2 + \gamma^2 v^2 R_{\parallel}^2 + \frac{1}{\beta_{\perp}^2} R_{\perp}^2, \quad (42)$$

$$B' = \gamma^2 R_{\parallel}^2 + \gamma^2 v^2 R_0^2 + \frac{\beta_l^2}{\beta_{\perp}^2} R_{\perp}^2, \quad (43)$$

$$C' = (R_0^2 + R_{\parallel}^2) \gamma^2 v + \frac{\beta_l}{\beta_{\perp}^2} R_{\perp}^2. \quad (44)$$

In Appendix A we show that the Modified YKP parametrization is defined everywhere except for the point $K_{\perp} = 0$ to which it can be smoothly extrapolated. Furthermore, whereas the relative momentum components used in the original YKP parametrization satisfy the inequality

$$q_{\perp} \geq q_o = \frac{1}{\beta_{\perp}} q^0 - \frac{\beta_l}{\beta_{\perp}} q_l, \quad (45)$$

which means that the data points never fill the whole three-dimensional q -space, no such restriction exists for q_s which is used in the modified parametrization. This should help to avoid certain technical problems in the fitting procedure which can occur with the YKP parametrization [55]. In any case, it may be useful to check the YKP fit against a modified YKP fit via the relations (39)-(41), in order to avoid the pitfalls related to the possible non-existence of a YKP parametrization for the data under study (which may not show up clearly in the fitting process but cause it to converge to a wrong result).

Unfortunately, the physical interpretation of the modified YKP radii is no more as straightforward as that of the original ones. Wherever in A, B, C the difference $\langle \tilde{x}^2 - \tilde{y}^2 \rangle$ occurs it is now replaced in A', B', C' by $\langle \tilde{x}^2 \rangle$ alone. For transparent sources the difference $\langle \tilde{x}^2 - \tilde{y}^2 \rangle$ is usually small [20] and the corresponding correction terms to the leading geometric contributions to R_0^2 and R_{\parallel}^2 are of minor importance; this permits a direct interpretation of R_0 and R_{\parallel} as the effective lifetime and longitudinal size of the source in its own rest frame [19]. For such sources the occurrence of $\langle \tilde{x}^2 \rangle$ alone in the modified radius parameters is certainly a drawback and usually leads to large corrections which invalidate a naive geometrical space-time interpretation (see Fig. 14). For opaque sources the appearance of $\langle \tilde{x}^2 \rangle$ (which is related to the curvature

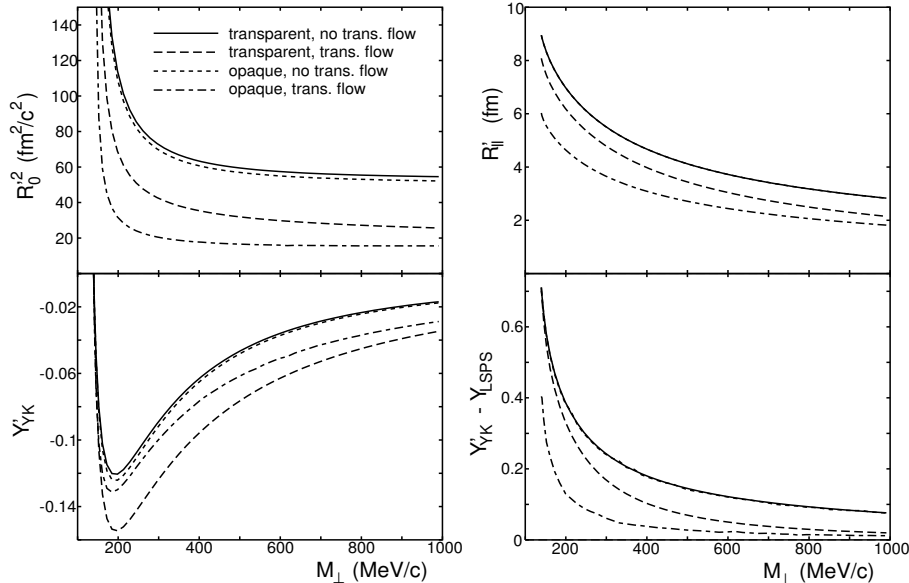


Figure 14: The correlation radii R'_0 and R'_{\parallel} of the Modified YKP parametrization, for pions at $Y_{\text{CM}} = 1.5$. Solid and dashed lines correspond to a transparent source with $\eta_f = 0$ (solid) and $\eta_f = 0.6$ (dashed). Dotted and dash-dotted lines correspond to an opaque source with $\lambda = R/14$, again with $\eta_f = 0$ (dotted) and $\eta_f = 0.6$ (dash-dotted). The lower row shows the modified Yano-Koonin rapidity Y'_{YK} in the LCMS (left) and relative to the LSPS (right) as a function of M_{\perp} . Source parameters as in Table 1.

and thickness of the emitting surface shell) instead of the generically much larger combination $\langle \tilde{x}^2 - \tilde{y}^2 \rangle$ may at first sight appear as an advantage. Nevertheless, unless

the emitting surface layer is indeed *very* thin (and very flat!), the resulting correction term in particular to the leading contribution in R'_0 cannot be neglected and spoils its simple interpretation as an effective source lifetime. This is shown in the left upper panel of Fig. 14; even for opaque sources with a rather small mean free path $\lambda = R/14$, one sees that R'_0 is much bigger than the effective source lifetime $\Delta\tau = 2 \text{ fm}/c$, even at large values of M_\perp (where $\beta_\perp \approx 1$) and for sources both with and without transverse expansion.

The effects on the modified longitudinal radius parameter R'_\parallel (right upper panel in Fig. 14) are much smaller, due to the small value of the longitudinal pair velocity β_l in the modified YK frame (where $v' = 0$) which multiplies the correction terms. β_l is small in the modified YK frame because, like the original YK rapidity, Y'_{YK} rises linearly with the pair rapidity Y_{CM} with nearly unit slope, reflecting the boost-invariant longitudinal expansion of the source (see upper row of Fig. 15). The difference between Y'_{YK} and

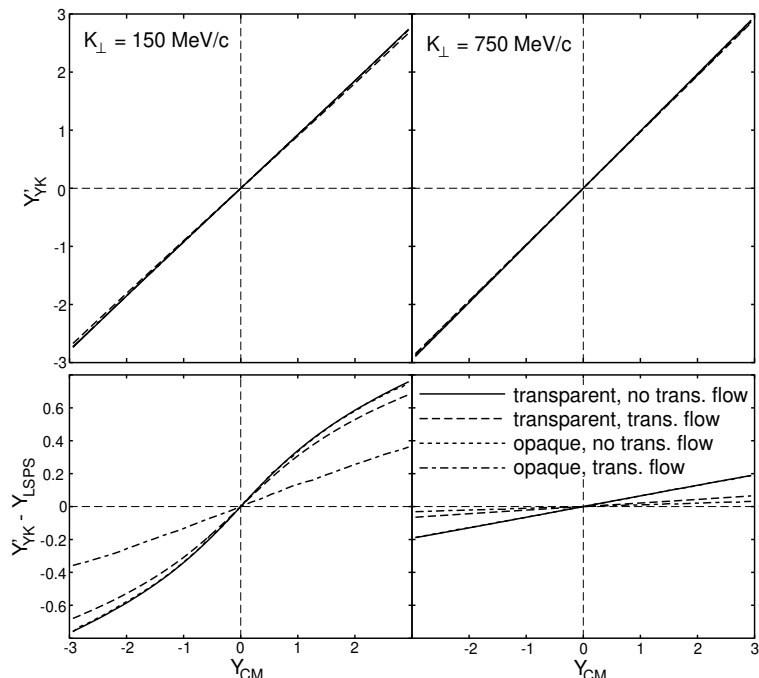


Figure 15: The modified YK rapidity Y'_{YK} in the LCMS (upper row) and relative to the LSPS (lower row) as a function of the pion pair rapidity in the CMS, for two values of K_\perp : 100 MeV/c (left) and 750 MeV/c (right). Line symbols as in Fig. 14.

the longitudinal flow rapidity Y_{LSPS} around the point of maximum emissivity (see lower row of Fig. 15) is somewhat larger than for the original YK rapidity for transparent sources [19, 20], but still small enough to consider Y'_{YK} as a good approximation for the rapidity of the effective source. The difference between Y'_{YK} and the rapidities of the LCMS and LSPS disappears in the limit $K_\perp \rightarrow \infty$, as for the original YK rapidity. Opacity effects on Y'_{YK} are seen to be small.

6 Conclusions

Let us shortly summarize the most important results:

Transverse temperature gradients and transverse flow have similar effects on the transverse HBT radii $R_s = R_\perp$, but not on the single particle spectra. Both lead to a decrease of R_s with increasing M_\perp , but while transverse flow flattens the single particle spectra, a transverse temperature gradient only reduces their normalization. A weak M_\perp -dependence of R_s due to a moderate transverse flow can be *increased* by adding a transverse temperature gradient, but only at the expense of simultaneously *reducing* the flow effects on the single particle spectra. This is important for the interpretation of experimental data.

For transparent sources, transverse temperature gradients preserve the M_\perp -scaling of the YKP radius parameters while transverse flow breaks it. This breaking of M_\perp -scaling is weak, however, the most sensitive parameter being R_0^2 .

Temporal temperature gradients affect mostly the temporal HBT radii, i.e. the difference $R_o^2 - R_s^2$ in the Cartesian parametrization and R_0^2 in the YKP parametrization.

We could not confirm the existence of a common $1/\sqrt{M_\perp}$ scaling law for all three Cartesian HBT radius parameters and the effective source lifetime in the case of the “thermal lengths” being smaller than the geometric lengths. For realistic model parameters, the M_\perp -dependence for R_s and R_0 is always much weaker than for the longitudinal radius parameters R_l resp. R_\parallel .

Opacity of the source was found to have dramatic effects on the YKP radius parameter R_0^2 . Opacity was parametrized in terms of the ratio between the surface thickness or mean free path λ and the transverse fireball radius R . Even for moderate values of $\lambda/R \sim 1$, a strong breaking of the M_\perp -scaling can be observed in the “temporal” YKP radius R_0^2 . Furthermore, R_0^2 becomes negative, especially so for small values of K_\perp . This feature extends over the larger a range in M_\perp the smaller the ratio λ/R . For $\lambda/R < 1$ the effect should be clearly visible in existing data from Pb-Pb collisions at CERN. Since it is not seen the experiments favor a source with volume-dominated particle emission.

Our investigation of opaque sources has led us to the discovery of previously unknown regions of inapplicability of the YKP parametrization for the correlation function. They are connected with the use of $q_\perp = \sqrt{q_s^2 + q_o^2}$ instead of q_s as an independent relative momentum variable. We found that for strongly opaque sources the YK velocity may become ill-defined. For this situation we suggested a modified YKP parametrization which is always well-defined and particularly suited for opaque sources. It can always be used as a technical tool to check the correct convergence of the YKP fit, by using the relations (39)-(41). On the physical level, the modified YK velocity v' can again be interpreted, in good approximation, as the longitudinal velocity of the effective source. It continues to reflect the longitudinal expansion of the source through a strong dependence on the rapidity of the emitted pairs. The interpretation of the modified transverse and longitudinal radius parameters R'_\perp and R'_\parallel as transverse and longitudinal regions of homogeneity in the source rest frame remains valid with sufficient approximation. The interpretation of $R_0'^2$ (which is now always positive) as the square of the effective source lifetime, however, is spoiled by a large geometric correction. The extraction of a reliable estimate of the source lifetime for opaque sources thus appears to be a very difficult problem.

Acknowledgments: We are indebted to Ján Pišút, Claus Slotta and Urs Wiedemann for valuable and helpful comments. We also thank Harry Appelshäuser, Tamas Csörgő, and Axel Vischer for discussions which partially motivated this work. We acknowledge financial support by DAAD, DFG, BMBF, and GSI.

A Definition range for the YKP parameters

The Yano-Koonin velocity v in Eq. (14) is only defined if the discriminant

$$D = (A + B)^2 - 4C^2 \quad (46)$$

is positive. Here we study the conditions under which this is the case. To this end we rewrite the expressions (11)-(13) as

$$A = \langle \tilde{t}^2 \rangle - \frac{2}{\beta_\perp} \langle \tilde{t} \tilde{x} \rangle + \frac{1}{\beta_\perp^2} \langle \tilde{x}^2 \rangle - \frac{1}{\beta_\perp^2} \langle \tilde{y}^2 \rangle = A' - \frac{1}{\beta_\perp^2} \langle \tilde{y}^2 \rangle, \quad (47)$$

$$B = \langle \tilde{z}^2 \rangle - 2 \frac{\beta_l}{\beta_\perp} \langle \tilde{z} \tilde{x} \rangle + \frac{\beta_l^2}{\beta_\perp^2} \langle \tilde{x}^2 \rangle - \frac{\beta_l^2}{\beta_\perp^2} \langle \tilde{y}^2 \rangle = B' - \frac{\beta_l^2}{\beta_\perp^2} \langle \tilde{y}^2 \rangle, \quad (48)$$

$$C = \langle \tilde{z} \tilde{t} \rangle - \frac{\beta_l}{\beta_\perp} \langle \tilde{t} \tilde{x} \rangle - \frac{1}{\beta_\perp} \langle \tilde{z} \tilde{x} \rangle + \frac{\beta_l}{\beta_\perp^2} \langle \tilde{x}^2 \rangle - \frac{\beta_l}{\beta_\perp^2} \langle \tilde{y}^2 \rangle = C' - \frac{\beta_l}{\beta_\perp^2} \langle \tilde{y}^2 \rangle. \quad (49)$$

We then have

$$A' = \left\langle \left(\tilde{t} - \frac{1}{\beta_\perp} \tilde{x} \right)^2 \right\rangle \geq 0 \quad (50)$$

$$B' = \left\langle \left(\tilde{z} - \frac{\beta_l}{\beta_\perp} \tilde{x} \right)^2 \right\rangle \geq 0 \quad (51)$$

$$C' = \left\langle \left(\tilde{t} - \frac{1}{\beta_\perp} \tilde{x} \right) \left(\tilde{z} - \frac{\beta_l}{\beta_\perp} \tilde{x} \right) \right\rangle \quad (52)$$

and thus

$$|A' + B'| = A' + B'. \quad (53)$$

We will prove that

$$(A' + B')^2 - 4C'^2 \geq 0 \quad (54)$$

or

$$|A' + B'| - 2|C'| \geq 0. \quad (55)$$

Due to (53) the inequality (55) can be written as

$$A' + B' \mp 2C' \geq 0 \quad (56)$$

where the upper sign stands for $C' > 0$ and the lower for $C' < 0$. Inserting expressions (50)-(52) we obtain

$$A' + B' \mp 2C' = \left\langle \left\{ \left(\tilde{t} - \frac{1}{\beta_\perp} \tilde{x} \right) \mp \left(\tilde{z} - \frac{\beta_l}{\beta_\perp} \tilde{x} \right) \right\}^2 \right\rangle \geq 0. \quad (57)$$

This proves (54). Since A' , B' , and C' are the shorthands belonging to the modified YKP parametrization, we have also proven that this parametrization is defined everywhere (except, of course, the point $K_\perp = \beta_\perp = 0$ [19, 20]).

From expressions (47-49) we see that

$$A + B = A' + B' - \frac{1 + \beta_l^2}{\beta_\perp^2} \langle \tilde{y}^2 \rangle \quad (58)$$

$$2C = 2C' - \frac{2\beta_l}{\beta_\perp^2} \langle \tilde{y}^2 \rangle. \quad (59)$$

It is therefore possible to obtain negative values for D :

$$D = (A + B)^2 - 4C^2 < 0. \quad (60)$$

For example, if $\beta_l = 0$ and $\langle \tilde{y}^2 \rangle$ is fixed at a value bigger than $\langle \tilde{x}^2 \rangle$, one can find values for β_\perp such that

$$|A + B| = \left| A' + B' - \frac{1}{\beta_\perp^2} \langle \tilde{y}^2 \rangle \right| < 2|C'| = 2|C|. \quad (61)$$

We must therefore conclude that there are kinematical regions where the YKP parametrization is not defined.

References

- [1] R. Hanbury Brown and R.Q. Twiss, Phil. Mag. **45**, 633 (1954); and Nature **177**, 27 (1956); **178**, 1046 (1956); **178**, 1447 (1956).
- [2] G. Goldhaber, S. Goldhaber, W. Lee, and A. Pais, Phys. Rev. **120**, 300 (1960).
- [3] M. Gyulassy, S.K. Kauffmann, and L.W. Wilson, Phys. Rev. C**20**, 2267 (1979).
- [4] B. Lörstad, Int. J. Mod. Phys. A**12**, 2861 (1989).
- [5] D. Boal, C.K. Gelbke and B. Jennings, Rev. Mod. Phys. **62**, 553 (1990).
- [6] W.A. Zajc, in: *Particle Production in Highly Excited Matter*, edited by H.H. Gutbrod and J. Rafelski, (Plenum Press, New York, 1993), p. 435.
- [7] S. Pratt, in: *Quark-Gluon Plasma 2*, edited by R.C. Hwa, (World Scientific Publ. Co., Singapore, 1995), p. 700.
- [8] U. Heinz, in: *Correlations and Clustering Phenomena in Subatomic Physics*, edited by M.N. Harakeh, O. Scholten, and J.H. Koch, NATO ASI Series B, (Plenum, New York, 1997) (Los Alamos eprint archive nucl-th/9609029).
- [9] A.N. Makhlin and Y.M. Sinyukov, Z. Phys. C**39**, 69 (1988).
- [10] S. Chapman, P. Scotto, and U. Heinz, Phys. Rev. Lett. **74**, 4400 (1995).
- [11] S. Chapman, P. Scotto, and U. Heinz, Heavy Ion Physics **1**, 1 (1995).

- [12] U.A. Wiedemann, P. Scotto and U. Heinz, Phys. Rev. C**53**, 918 (1996).
- [13] T. Csörgő and B. Lörstad, Nucl. Phys. A**590**, 465c (1995).
- [14] T. Csörgő and B. Lörstad, Phys. Rev. C **54**, 1390 (1996).
- [15] T. Csörgő and B. Lörstad, in *Proceedings of XXV International Symposium on Multiparticle Dynamics*, Sept. 12.-16. 1995, Stará Lesná, Slovakia, edited by D. Bruncko, L. Šándor and J. Urbán (World Scientific, Singapore, 1996), p. 661.
- [16] S.V. Akkelin and Y.M. Sinyukov, Z. Phys. C**72**, 501 (1996).
- [17] H. Heiselberg and A.P. Vischer, Los Alamos eprint archive nucl-th/9609022.
- [18] H. Heiselberg and A.P. Vischer, Los Alamos eprint archive nucl-th/9703030.
- [19] U. Heinz, B. Tomášik, U.A. Wiedemann, and Y.-F. Wu, Phys. Lett. B**382**, 181 (1996).
- [20] Y.-F. Wu, U. Heinz, B. Tomášik, and U.A. Wiedemann, Los Alamos eprint archive nucl-th/9607044, Z. Phys. C, in press.
- [21] B. Tomášik, U. Heinz, U.A. Wiedemann, and Y.-F. Wu, Acta Phys. Slovaca **47**, 81 (1997).
- [22] T. Csörgő, P. Lévai, and B. Lörstad, Acta Phys. Slovaca **46**, 585 (1996).
- [23] T. Csörgő and B. Lörstad, Heavy Ion Physics **4**, 221 (1996).
- [24] NA44 Coll., H. Beker et al., Phys. Rev. Lett. **74**, 3340 (1995).
- [25] NA35 Coll., T. Alber et al., Z. Phys. C **66**, 77 (1995);
NA35 Coll., T. Alber et al., Phys. Rev. Lett. **74**, 1303 (1995).
- [26] T. Alber, PhD thesis, MPI für Physik, München (1995), unpublished.
- [27] T. Alber for the NA35 and NA49 Coll., Nucl. Phys. A **590**, 453c (1995).
- [28] K. Kadija for the NA49 Coll., Nucl. Phys. A **610**, 248c (1996).
- [29] S. Schönfelder, PhD thesis, MPI für Physik, München, 1996, unpublished.
- [30] H. Appelhäuser, PhD thesis, Johann Wolfgang Goethe-Universität Frankfurt/Main, 1996, unpublished.
- [31] S. Chapman, J.R. Nix, and U. Heinz, Phys. Rev. C**52**, 2694 (1995).
- [32] F. Yano and S. Koonin, Phys. Lett. B**78**, 556 (1978).
- [33] M.I. Podgoretskii, Sov. J. Nucl. Phys. **37**, 272 (1983).
- [34] B. Schlei and U. Heinz, in preparation.
- [35] J. Bolz et al., Phys. Lett. B**300**, 404 (1993); and Phys. Rev D**47**, 3860 (1993).
- [36] B.R. Schlei et al., Phys. Lett. B**376**, 212 (1996).

- [37] U. Ornik et al., Los Alamos eprint archive hep-ph/9604323.
- [38] H. Heiselberg, Phys. Lett. **B379**, 27 (1996).
- [39] T. Csörgő, B. Lörstad, and J. Zimányi, Z. Phys. C**71**, 491 (1996).
- [40] U.A. Wiedemann and U. Heinz, Los Alamos eprint archive nucl-th/9611031, submitted to Phys. Rev. C.
- [41] U.A. Wiedemann and U. Heinz, Los Alamos eprint archive nucl-th/9610043.
- [42] U.A. Wiedemann and U. Heinz, Acta Phys. Slovaca **47**, 95 (1997).
- [43] E. Shuryak, Phys. Lett. B**44**, 387 (1973); Sov. J. Nucl. Phys. **18**, 667 (1974).
- [44] S. Pratt, Phys. Rev. Lett. **53**, 1219 (1984); Phys. Rev. D**33**, 1314 (1986).
- [45] S. Chapman and U. Heinz, Phys. Lett. B**340**, 250 (1994).
- [46] M. Herrmann and G.F. Bertsch, Phys. Rev. C**51**, 328 (1995).
- [47] T. Csörgő and S. Pratt, in *Proceedings of the Workshop on Relativistic Heavy Ion Physics at Present and Future Accelerators*, Budapest, 1991, edited by T. Csörgő et al. (MTA KFKI Press, Budapest, 1991), p. 75.
- [48] J.D. Bjorken, Phys. Rev. D**27**, 140 (1983).
- [49] U. Heinz, Nucl. Phys. A**610**, 264c (1996).
- [50] S. Chapman and J.R. Nix, Phys. Rev C**54**, 866 (1996).
- [51] U. Heinz, B. Tomášik, and U.A. Wiedemann, work in progress.
- [52] K.S. Lee, U. Heinz, and E. Schnedermann, Z. Phys. C**48**, 525 (1990); E. Schnedermann, J. Sollfrank, and U. Heinz, Phys. Rev. C**48**, 2462 (1993).
- [53] Proceedings from *Quark Matter '96*, (Heidelberg, 20.-24.5.1996), edited by P. Braun-Munzinger et al., Nucl. Phys. A **610** (1996).
- [54] P.J. Siemens and J.O. Rasmussen, Phys. Rev. Lett. **42**, 880 (1979).
- [55] B. Lasiuk, Acta Phys. Slovaca **47**, 15 (1997).